Electroosmotic Sampling and Its Application to Determination of Ectopeptidase Activity in Organotypic Hippocampal Slice Culture when coupled with HPLC-EC

by

Hongjuan Xu

BS, Nanjing University, P. R. China, 2000

MS, Nanjing University, P. R. China, 2003

Submitted to the Graduate Faculty of the

Dietrich School of Arts and Sciences in partial fulfillment

of the requirements for the degree of

Doctor of Philosophy

University of Pittsburgh
2013

UNIVERSITY OF PITTSBURGH

Dietrich School of Arts and Sciences

This dissertation was presented

by

Hongjuan Xu

It was defended on

MARCH 1, 2013

and approved by

Arian C. Michael, Ph.D., Professor of Chemistry

Shigeru Amemiya, Ph.D., Professor of Chemistry

Billy W. Day, Ph.D., Professor of Chemistry and Pharmaceutical Sciences

Stephen G. Weber, Ph.D., Professor of Chemistry and Clinical & Translational Sciences

Electroosmotic Sampling and Its Application to Determination of Ectopeptidase Activity in Organotypic Hippocampal Slice Culture when Coupled with HPLC-EC

Hongjuan Xu, Ph.D.

University of Pittsburgh, 2013

Abstract

Sampling through extracellular space has always been a challenge. Traditional methods, such as push-pull perfusion, microdialysis and direct sampling, are not suitable for sampling through thin slice cultures; since they all involve probe implantation. Through this research we developed a novel sampling method based on electroosmosis. By taking advantage of the natural ζ-potential in an organotypic hippocampus slice culture, an electroosmotic flow was successfully invoked within the extracellular space by applying an electric field. This flow was used to draw the physiological fluid from the slice culture. We have characterized this method by examining the flow rate, sampling bias, internal standard and damage caused during sampling. Coupled with a capillary high performance liquid chromatography (HPLC) and an electrochemical detection, this novel sampling method was applied to study enkephalin hydrolysis by ectoenzymes distributed in the hippocampus area. The results showed not only the feasibility and efficiency of the electroosmotic sampling technique in extracting extracellular material, but also its potential for studying ectopeptidase activity. A capillary Taylor reactor was employed to perform post-column reactions in the electrochemical detection. This reactor shares pressure with the capillary column and adds band-spreading, which reduce separation efficiency. We quantitatively evaluated this effect and gave a set of optimal and practical conditions.

Acknowledgement

I would like to express my sincere gratitude to Dr. Stephen G Weber, my advisor for his guidance, encouragement, trust, patience and consideration during my graduate research. He has provided a very free research environment. He always inspires me with novel ideas and encourages me to solve problems. He respects and fully supports the choices I have made during my study in Pittsburgh. I really appreciate that he encouraged and helped me not to give up but to face my difficulties in finishing my dissertation. His diligence and passion in science and his attitude to life has benefitted me during my graduate research and will continue to do so in my future career and life as well.

I would like to thank Dr. Billy Day, Dr. Adrian Michael and Dr. Shigeru Amemiya for their constant help during my graduate studies. Thanks for serving on my committee. I learned a lot through conversation with them.

It has been a wonderful experience to work with my intelligent colleagues in Weber group. I have learned a lot from them in group meetings and through discussing with them on various experimental problems. I am thankful for their friendship and encouragement.

Last but not the least, I want to give thanks to my husband, Hongjun Yue, my son, Alan Yue and my parents. They are the joy of my life. They have always been there for me whenever I needed them. They unconditionally support me, love me and sometimes even spoil me. I am grateful for their love. Without them, I could not finish this thesis.

Table of Contents

List of Figures

List of Tables

Chapter 1 Introduction

Neuropeptides play key roles in the function of brain and peripheral nervous system such as pain and learning[1]. They are mainly inactivated by ectopeptidases which are membrane bound with their active sites facing extracellular space. These enzymes cleave active neuropeptides into inactive fragments[2-4]. For example, thyrotropin-releasing hormone (TRH), an important extracellular signal substance, is inactivated after released by an ectoenzyme which locates preferentially on neuronal cells in the brain and on lactotrophic pituitary cells[5]. Angiotensin-converting enzyme (ACE), aminopeptidase N (APN) and endopeptidase 24.11 have been determined to regulate the metabolism and biological function of CRF (the corticotrophin-releasing factor)[6]. Ectopeptidases are also involved in the hydrolysis of opioid peptides such as enkephalins in the brain, kidney and intestines[7]. Moreover, membrane peptidases play important roles in cell activation, proliferation and communication. Thus, in-deep understanding of ectopeptidase activity is necessary for understanding both normal and pathological brain function as well as for designing novel strategies for drug development. A major concern of the analysis of ectopeptidase activity is tissue fractionation or damage which releases the cytosolic peptidases that interfere with the analysis by contributing to peptide degradation. Reliable analysis of ectopeptidase activity requires intact cells or tissues.

1.1 Current Methods in Peptidase Analysis

Most of our knowledge of peptidases came from the analysis of tissue extracts, homogenate or fraction by determination of peptide fragment using HPLC[8, 9] or standard enzyme methods (fluorogenic substrate)[10, 11]. Although these methods offer experimental simplicity, they suffer the interference from cytosolic peptidases and membrane bound peptidases facing intracellularly which degrade peptide also. For this reason, conventional methods are not favorable for ectopeptidase analysis. Another limitation of these methods is the lack of spatial resolution. A good spatial resolution is necessary in some cases. For instance, enkephalin-degrading activity has a co nsiderable variation across the human brain[12]. Another common method is to simply incubate the target tissue culture into substrate solution and then analyze the solution. This method relies on slow diffusion thus resulting in a poor time resolution.

Microdialysis is actively used in peptidase analysis. Peptidase activity has been a concern in microdialysis experiments. Microdialysis sampling of peptides is improved in the presence of peptidase inhibitors[13-19]. Continuous sampling of neuropeptides and monitoring their concentrations in exctracellular space help us understand the ectopeptidase activity. Quantification of neuropeptides in dialysates is challenging due to their low extracellular concentrations (low pM range), their low microdialysis efficiencies, the need for acceptable temporal resolution, the small sample volumes, the complexity of cell matrix and the tendency of peptides to stick to glass and the polymeric membrane of a microdialysis probe[20].

Many efforts have been made to overcome these problems. A number of LC-MS/MS and microdialysis parameters have been optimized to achieve maximum sensitivity so that *in vivo* neuropeptide release can be investigated[20]. Microdialysis sampling combined with LC-ESI-MS detection allowed for *in situ* determination of the enzymatic activity of a protease external to the

microdialysis probe when using different peptide-based substrates[21]. Non-specific binding of peptides to the tubing and probe membrane limits microdialysis to evaluate the absolute extracellular concentrations. A systematic approach for reducing and evaluating the non-specific binding has strengthened the applicability of microdialysis[22]. However, this evaluation has to be made *in vitro* in each individual case before *in vivo* microdialysis. It is complicated since a range of additives in perfusion fluid and tubing material has to be tested *in vitro*. New tubing material, probe membrane and additives might improve or resolve the non-specific binding issues. Microdialysis is an established technique for sampling small molecules through extracellular space but not for collecting larger molecules. Using a new "vent" probe with a push-pull perfusion system, pathophysiologically important macromolecules such as Aβ peptides are successfully sampled from the brain of a free-moving mouse with a constant recovery rate[23]. This novel system contains a polyethylene membrane probe (1000 kDa MWCO) and a push syringe and pull peristaltic pump simultaneously operated at various flow rates, which allows rapid equalization of the pressure inside the probe and results in constant recovery rates.

Overall, microdialysis is a well established and powerful technique. It finds its application in the peptidase or protease activity due to its capacity in real-time observation of concentration changes in extracellular space[24-27]. However, microdialysis also has some disadvantages. The time resolution in many cases is over 10 min as the flow rate of perfusate is low (usually less than 2 μL/min). The low time resolution is also related to the detection limits of the coupled analytical method. In ordinary conditions, peptide concentration in the dialysate is around 5% or less. Detection becomes much more challenging due to such dilution. Furthermore, the spatial resolution of microdialysis is limited by the length of the semipermeable membrane

which is usually 2-4 mm. Implanting the probes causes a penetration injury in the brain tissue[28-29].

1.2 Our Approach

We have developed a novel sampling method based on electroosmosis, which is more suitable for neurochemical extraction from the extracellular space in slice cultures. We demonstrated the feasibility and advantages of this electroosmosis sampling in ectopeptidase activity studies when coupled with HPLC-EC. In this research, we used organotypic hippocampal slice culture as an experimental model and applied Leu-enkephaline (YGGFL) degradation as an experimental probe. The following gives a detailed background related to this study.

1.2.1 Organotypic Hippocampal Slice Culture (OHSC)

Slices derived from various brain regions are predominant *in vitro* preparations for studying the physiological and pharmacological properties of neuronal circuits. They are easy to prepare and they maintain the cytoarchitecture of the tissue of origin. However, acute slices are short-lived. For experiments that require long-term survival of the preparations, such as studies involving chronic application of neural connectivity, development of neural connectivity, fiber growth and synaptic transmission in co-cultures derived from different brain areas, acute slices are obviously not suitable. Thus, slice cultures have become an attractive alternative and a necessary complement to acute slices. Procedures have been developed to sustain brain tissues in culture. The most popular ones are the roller tube and interface techniques. Both produce organotypic

culture, a term introduced initially for neuronal cultures by C rain[30, 31] to describe the cytoarchitecture of explants which mimic their *in situ* counterparts.

Both techniques start from acute slices with desired thickness. In the roller tube technique [32-34] a slice is attached onto a glass coverslip by means of a chicken plasma clot or sometimes a collagen matrix and then put into a plastic test tube with enough medium. The test tube is placed in a roller drum. This continuous slow rotation ensures feeding and oxygenation of the culture because the culture is immersed in the medium for half a circle and covered by a film of medium for the other half circle in dry air. The culture is incubated at 36 ± 0.5 °C. Medium is exchanged weekly. In the interface preparation[35], a slice is positioned on a sterile, transparent and low protein binding PTFE porous membrane with culture medium underneath it. The insert is then put into an incubator with a temperature set to 36 °C and with a 5% CO_2-enriched atmosphere. The porous membrane surface provides an air/medium interface. Slices obtain sufficient nutrient and remain well exposed to air at the same time. The medium is exchanged twice a week.

Slice cultures yielded from both procedures share some characteristics: they duplicate the cytoarchitecture of their *in vivo* counterparts; slice cultures are flatten in medium; even after 2-3 weeks in culture, neurons still exhibit morphological as well as electrophysiological properties similar to what has found in slices of the same age; in culture, synaptic reorganization, sprouting or selection of cells by death of certain cell types may occur.

Without the lengthy process of coverslip cleaning, the use of chicken plasma clot or the slow rotation, interface preparation beats roller tube technique for simplicity. It only needs insert membranes and an incubator for culture. In the presence of plasma clot, studying events occurring during the first days in culture such as synaptic reorganization is difficult. In contrast, such studies are facilitated on slice cultures grown in membrane culture method, since an insert

membrane is transparent and has no autofluorescence. Cultures prepared from the membrane culture method flatten considerably during the first week but still maintain the thickness of a few cell layers, while those from the roller tube technique shrink to a monolayer thick over a great area. With increase in culturing time, the plasma clot that surrounds the tissue is progressively lysed away, leaving monolayer thick tissue directly on the coverslip. This monolayer characteristic obviously favors the visualization and accessibility of individual living cells. Tissues cultured by filter membrane technique show reduced gliosis in comparison to those cultured by roller tube technique, suggesting the long term culture brain tissues may fare better on membrane.

Both methods have been utilized to culture and co-culture tissues derived from various regions of postnatal rat brains. Lack of extensive application suggests the difficulties of culturing slices from adult rat brain even though some researchers have made many efforts to improve the survival. Nevertheless, researchers[36] have found the possible application of slice cultures from adult rat brain in the studies of age related neuronal degeneration and testing of neuroprotective compounds. They found that the cell death in the adult slice culture (specifically OHSCs) is time-dependent and reproducible.

We chose interface preparation of OHSC in this research. OHSC has been used as a model to study neuroprotection against all sorts of neuronal cell damage induced by excitotoxins such as NMDA and kainic acid and by oxygen-glucose deprivation caused ischemia. It also has applications in studies of synaptic plasticity and neurogenesis.

Hippocampus plays an important role in long-term memory and learning. Hippocampus is also highly susceptible to seizure and vulnerable to the effect of ischemia and anoxia. After a couple of weeks of culturing, OHSCs mimic many aspects of their *in vivo* counterparts. The local

synaptic contacts are still functional and the structure of hippocampus is well preserved. Each OHSC contains a laminar of the hippocampus structure.

Compared to whole animal modes, slice culture based assay allows easier experimental access which is time-saving especially for studies involving screening of therapeutic molecules or novel genes. It also gives better control of the extracellular environment than is possible *in vivo* so that the biological outcomes can be simply elucidated, which is favorable for ectopeptidase activity studies. The thickness of an OHSC has been measured in our laboratory to be 148 ± 8 μm with an initial thickness of 400 μm after 6-8 days in culture[37]. Microdialysis or push-pull sampling is hard to apply to such a thin slice culture.

1.2.2 The Feasibility of Sampling Based on Electroosmosis

Cell membrane and extracellular matrix components include phospholipid head groups, proteins and sulfated carbohydrates. These components ionize in the presence of an electrolyte solution such as cerebrospinal fluid. The charges that originate from the cell surfaces and the immobile extracellular matrix affect the distribution of ions in the extracellular fluid (counter ions with an increased concentration close to the cell surface) and result in the development of an electrical double layer (Stern layer or compact layer and diffuse layer). Ions in the Stern layer are strongly bound to the cell surface while those in the diffuse layer are less firmly attached. The ζ-potential is the electric potential at the slip plane between the mobile and stationary ions. The ζ-potential of an OHSC has been measured in our laboratory to be -22 mV[38].

Electroosmotic flow is the motion of liquid induced by an external electric field applied to a porous material, capillary tube, membrane or any other fluid conduit with fixed charges on

the surface and a moving electrolyte solution adjacent to it. The magnitude of electroosmotic flow depends linearly on the magnitude of ζ-potential as expressed in Equation (1)

$$v_{eo} = -(\varepsilon\zeta/\eta)E \qquad (1)$$

where ε is the permittivity and η is the viscosity of the medium. An OHSC has a ζ-potential of -22 mV, suggesting that electroosmotic flow containing extracellular solutes will be generated in the extracellular space once an electric field is applied.

For a charged species, v_{obs} is not equal to v_{eo}. It is the sum of electroosmotic and electrophoretic velocity. The latter is defined in Equation (2).

$$v_{ep} = (\varepsilon\zeta_{particle}/\eta)E \qquad (2)$$

Where $\zeta_{particle}$ is the ζ-potential defined by the surface charge on the particle. Thus, the observed velocity of a charged species can be expressed in Equation (3).

$$v_{obs} = v_{eo} + v_{ep} = -\left(\frac{\varepsilon\zeta}{\eta}\right)E + \left(\frac{\varepsilon\zeta_{particle}}{\eta}\right)E \qquad (3)$$

When the two velocities are in opposite directions and of the same magnitude, the species does not flow. This will be the case for us when the sampled species is negatively charged. In other words, electroosmotic sampling may not be feasible for negatively charged species with a high electrophoretic mobility.

1.2.3 Enkephalins and Their Degrading Enzymes

We picked enkephalin degradation as the experiment probe because the separation of hydrolysis products of enkephalin is well established in our lab. The enkephalinases are localized in some

brain regions including the hippocampus. And many literatures are available on these pepitdases and their inhibitors, although most of the work has been done by slice homogenization or whole slice incubation experiment.

Endogenous opiate system has been considered to be involved in a remarkable number of biofunctions. Enkephalins (Tyr-Gly-Gly-Phe-Met and Tyr-Gly-Gly-Phe-Leu), the first isolated endogenous opioid peptides, together with endorphins, dynorphins and orphanin compose the family of pain killing opioid peptides.

It is believed that enkephalins are involved in a number of physiological functions, such as pain perception and analgesia, regulating emotions, responding to stress and ethanol exposure, and modulating social behavior[39-43].

Enkephalins are mainly degraded by ectopeptidases[42-48]. In the central nervous system (CNS), there are several peptidases acting upon enkephalins at various amide sites. Most of these peptidases are not located right at the enkephalinergic synapses where enkephlins are released. Therefore, the inactivation of enkephalins occurs in the extracellular space. There are about seven ectopeptidases showing activity of enkephalin hydrolysis[44].

Aminopeptidase N (APN) hydrolyses enkephalin by removing the N-terminal tyrosine. Immunohistochemistry results clearly indicate that this peptidase activity is primarily localized in blood vessels[45]. APN is distributed throughout the cerebral cortex, enriched in the caudate and moderately expressed in the hippocampus. Bestatin at 15 μM inhibits greater than 90% of this aminopeptidase activity. APN is less sensitive to puromycin. Puromycin at 25 μM inhibits less than 20 % of the enzyme activity[42]. Blood vessels associated APN is likely to contribute most of the enkephalin hydrolysis activity found in brain homogenates[46].

Puromycin-senstive aminopeptidase (PSA), a ubiquitous enzyme, splits YGGFL at the Tyr-Gly peptide bond. Its concentration is the highest in the brain. Eighty percent of PSA present in cytosol and the rest is associated with membranes. But those membrane-bound PSAs mainly have their active sites facing intracellularly. Therefore PSAs are unlikely to function as ectopeptides.

Neural aminopeptidase (NAP), a neuronal specific peptidase, was detected in rats only in the brain, spinal cord and olfactory bulb, but not in peripheral tissues[44]. It also has heterogeneous distribution in the CNS with the highest activity in the hippocampus and lowest in the olfactory bulb. It is only 28% as active as PSA in hippocampus (which accounts for 59% of the total brain aminopeptidase activity) and only 14% as active as P SA in the olfactory bulb. Eighty five percent of this neural specific peptidase is soluble and the rest is membrane associated. This peptidase is absent in glioma C6 and neuroblastoma SK-N-SH cells which indicates that the enzyme is unique to the CNS neurons. NAP is susceptible to aminopeptidase inhibitors including actinonin, arphamenine B, probestatin, and H-borePheC6H12. It is most sensitive to amastatin with a K_i of 0.04 μM, followed by bestatin (0.19 μM), proctolin (0.76 μM), puromycin (0.95 μM) and Arg^0-enkephalin (4.75 μM). NAP is insensitive to the specific inhibitors of endopeptidase 24.11 (thiorphan), angiotensin (II) convertase (captopril) and carboxypeptidase (GEMSA), which is similar to PSA.

Neuron-specific aminopeptidase type 2 (NAP2) is similar to NAP. The majority (85%) of the activity of this neuronal aminopeptidase is found in cytosol and the rest is in the membranes[46]. It is also expressed exclusively in the CNS. NAP2 is most sensitive to amastatin with an IC_{50} of 0.05 uM. NAP2, NAP and PSA are also equally susceptible to bestatin (IC_{50} 0.2 μM) and proctolin (IC_{50} 0.8 μM). Puromycin works upon all three of these peptidases with a different IC_{50}.

NAP2 has regional activity distribution, more in the cerebral cortex than in the hippocampus, while NAP shows the highest activity in the hippocampus.

Angiotensin-converting enzyme (ACE) releases YGG from enkephalin. ACE has very low activity in three different cell cultures including neurons, astroblasts and astrocytes since its specific inhibitor, captopril, has little effect on the cleavage at Gly-Phe peptide bond[48]. ACE is mainly expressed in endothelial cells, which may be present in the primary cultures.

Dipeptidyl aminopeptidase (DAP) splits enkephalin to produce Tyr-Gly dipeptide. Its activity is much higher in neuronal than in the glial cultures. In the presence of bestatin, an inhibitor for aminopeptidase to prevent the degradation at Tyr-Gly position, Tyr-Gly becomes the main fragment in neuronal cultures, while Tyr-Gly-Gly is the main fragment in glial cultures. This aminopeptidase is present mainly in cytosol and its membrane bound activity is fairly low. Researchers even suspected that membrane-bound activity detected in experiments could be due to an intracellular enzyme which adsorbed to the cell membrane and leaked into the medium[48].

GEMSA is a specific inhibitor for carboxypeptidase which has very low activity (not even detectable) on both neuronal cells and glials cell as demonstrated[48]. Carboxypeptidase hydrolyzes Met-enkephalin at Phe-Met bond.

N4TG1 neuroblastoma cells, human endothelial cells, neuronal cells and astroblast cells from rat brains all have been demonstrated to hydrolyze enkephalins, mainly releasing the N-terminal Tyr. Therefore, aminopeptidases, splitting enkephalins at such a specific bond, are essential for the inactivation of enkephalin. A technique with improved spatial resolution and without perturbation from cytosolic enzymes or enzymes with active sites facing intracellularly will certainly help to clarify which peptidase is the most important for extracellular hydrolysis of enkephalin.

1.2.4 HPLC-EC System

HPLC is an essential separation approach for peptides. For biological samples with a total available volume of only a few microliters, suitable HPLC conditions can be achieved by reducing column diameter and the diameter of packing particles of the stationary phase which greatly shortens the distance from the bulk of the mobile phase to stationary phase surface. As the packing particle diameter decreases, both the A term and the C term in the van Deemter equation decease, but back pressure at constant velocity increases. The simultaneous application of columns packed by small particles and higher flow rates are enabled by high pressure pumps. Sub-2 μm packing particles with good thermal stability are commercially available. Smaller particle size combined with high flow rate and high temperature speeds up the HPLC analysis. High temperature decreases the viscosity of the mobile phase and accelerates mass transfer, both of which speed up HPLC separation.

HPLC can be coupled with antibody based binding assay, UV spectrophotometer, fluorescence, mass spectroscopy and electrochemical detection to complete the analysis of peptides. In this research, we chose electrochemical detection. Peptides with electroactive functional groups, W(Trp) and Y(Tyr), can be directly detected by an electrochemical detector. For those electrochemically silent peptides, the biuret reaction is used to convert them to electroactive derivatives[49]. Peptides longer than dipeptides react with Cu(II) to yield Cu(II)-peptide complexes which can be electrochemically oxidized to the corresponding Cu(III) complexes. This reaction is reversible. A downstream cathode can be used to detect Cu (III) complexes to improve the selectivity. This electrochemical detection coupled with biuret reaction gives a detection limit as low as a few nM. Under certain conditions and with peptide

concentration less than 1 μM, the HPLC-EC system gives baseline resolution for the peptide peak. Peak areas and peak heights are proportional to concentrations.

The derivatization process can be carried out pre-column or post-column[50]. There are some disadvantages of pre-column reaction. The reaction product has to be stable through the separation and detection process. The reaction might change the retention of the original forms of solutes so that the published separation procedure may not be directly adopted. Post-column reaction has its own problems. It requires additional hardware and reagents. It adds extra band broadening due to mixing following the separation. The band spreading issue has been addressed theoretically[51] as well as experimentally[52, 53]. We used a mixer, in conjunction with a fused silica capillary Taylor reactor (CTR) (a simple, open tube long enough to permit diffusional relaxation of radial concentration gradients), as a post-column reactor. The CTR has been demonstrated to have negligible effect on the separation of a capillary column at optimal conditions. Thus, it is well-suited to mix reagents with effluent from a capillary column.

We have demonstrated electroomostic sampling as a novel technique very suitable to extract extracellular fluid through a thin slice culture, which enables parallel experiments without sacrificing large numbers of animals. The spatial resolution has been assessed to be several hundreds of micrometers according to the area that is damaged during sampling (under extreme conditions). The spatial resolution is dependent on the inside diameter of the capillary; therefore it may be further improved by using a sampling capillary with a pulled tip. By controlling sampling time and electrical field strength, the sample dilution can be avoided. The temporal resolution might be highly improved when coupling electroosmotic sampling with other proper and sensitive detections, which will benefit the analysis of low-concentrated endogenous neuropeptides or neurotransmitters in specific brain areas. For instance, electroosmotic sampling

has been married with microfluidic chips and a co nfocal laser induced fluorescence (LIF) detector to successively sample, separate and detect the extracellular thiols in hippocampal tissue cultures[54].

Reference

1. Oegren, S. O.; Kuteeva, E.; Elvander-Tottie, E.; Hoekfelt, T. *Eur. J. Pharmacol.* **2009**, *626*, 9.
2. Kenny, A. J. *Peptidergic Neuron* **1996**, 87.
3. Konkoy, C. S.; Davis, T. P. *Trends Pharmacol. Sci.* **1996**, *17*, 288.
4. Roques, B. P. *Trends Pharmacol. Sci.* **2000**, *21*, 475.
5. Schauder B.; Schomburg L.; Kohrle J.; Bauer K. *Proc Natl Acad Sci USA* **1994**, 91, 9534.
6. Ritchie J. C.; Davis T.P.; Nemeroff C.B. *Neuropsychopharmacology* **2003**, 28, 22.
7. Miller B. C.; Ackrovd A.; Hersh L.B.; Cottam G.L. *Requl Pept.* **1994**, 50 (1), 87.
8. Ayyoub, M.; Monsarrat, B.; Mazarguil, H.; Gairin, J. E. *Rapid Commun. Mass Spectrom.* **1998**, *12*, 557.
9. Muller, S.; Ho, B.; Gambus, P.; Millard, W.; Hochhaus, G. *J. Pharm. Biomed. Anal.* **1997**, *16*, 101.
10. Bell Hannah, L.; Gooz, M. *Am. J. Med. Sci.* **2010**, 339, 105.
11. Brama, P. A. J.; TeKoppele, J. M.; Beekman, B.; Van El, B.; Barneveld, A.; Van Weeren, P. R. *Ann. Rheum. Dis.* **2000**, *59*, 155.
12. Mosnaim, A. D.; Nguyen, T. D.; Tse, R.; Puente, J.; Couceyro, P.; Wolf, M. E. *Neurochem. Res.* **2008**, *33*, 81.

13. Charli, J. L.; Mendez, M.; Vargas, M. A.; Cisneros, M.; Assai, M.; Joseph-Bravo, P.; Wilk, S. *Neuropeptides* **1989**, *14*, 191.

14. Kajiro, T.; Nakajima, Y.; Fukushima, T.; Imai, K. *Anal. Chem.* **2002**, *74*, 4519.

15. Littlewood, G. M.; Iversen, L. L.; Turner, A. J. *Biochem. Soc. Trans.* **1987**, *15*, 894.

16. Mauborgne, A.; Bourgoin, S.; Benoliel, J. J.; Hirsch, M.; Berthier, J. L.; Hamon, M.; Cesselin, F. *J. Pharmacol. Exp. Ther.* **1987**, *243*, 674.

17. Rose, C.; Vargas, F.; Silhouette, B.; Devaux, B.; Schwartz, J. C. *Neuropeptides* **1995**, *28*, 157.

18. Williams, J. T.; Christie, M. J.; North, R. A.; Roques, B. P. *J. Pharmacol. Exp. Ther.* **1987**, *243*, 397.

19. You, Z. B.; Nylander, I.; Herrera-Marschitz, M.; O'Connor, W. T.; Goiny, M.; Terenius, L. *Neuroscience (Oxford)* **1994**, *63*, 415.

20. Van Eeckhaut A.; Maes K.; Aourz N.; Smolders I.; Michotte Y. *Bioanalysis* **2011**, 3(11), 1271-85.

21. Wang Y.; Zagorevski, D.V.; Stenken J.A. *Anal.Chem.* **2008**, 80(6), 2050.

22. Nirogi R.; Kandikere V.; Bhyrapuneni G.; Benade V.; Saralaya R.; Irappanavar S.; Muddana N, Ajjala D.R. *J. Neurosci. Methods* **2012**, 209 (2), 379.

23. Takeda S.; Sato N.; Ikimura K.; Nishino H.; Rakugi H.; Morishita R. *Neuroscience* **2011**, 186, 110.

24. Kushikata T.; Hirota K. *Methods Mol. Biol.* **2011**, 789, 261.

25. Wang Y.; Zagorevski D.V.; Lennartz M.R.; Loegering D.J.; Stenken J.A. *Anal. Chem.* **2009**, 81, 9961.

26. Klintenberg, R.; Andren, P. E. *J. Mass Spectrom.* **2005**, *40*, 261.

27. Reed, B.; Zhang, Y.; Chait, B. T.; Kreek, M. J. *J. Neurochem.* **2003**, *86*, 815.

28. Borland, L.M *J. Neurosci. Methods* **2005**, 146(2), 149.

29. Yang, H.; Michael, A.C. *Electrochem. Methods Neurosci.* **2007**, 489.

30. Crain, S.M. *Int. Rev. Neurobiol*. **1966**, 9, 1.

31. Crain, S.M. *Neurophysiologic Studies in Tissue Culture*, Raven Press, New York, 595.

32. Gähwiler, B.H. *J.Neurobiol.* **1981**, 12, 187.

33. Gähwiler, B.H. *Proc.roy. Soc. B.* **1981**, 221, 287.

34. Gähwiler, B.H. *J. Neurosci. Methods* **1981**, 4, 329.

35. Stoppini, L.; Buchs, P. A.; Muller, D. *J Neurosci. Methods* **1991**, 37, 173.

36. Su, T.; Paradiso B.; Long, Y. S.; Liao W.P.; Simonato, M. *Brain Research* **2011**, 1385, 68.

37. Hamsher A.E.; Xu, H.; Guy, Y.; Sandberg, M.; Weber, S.G. *Anal. Chem.* **2010**, 82, 6370.

38. Guy, Y.; Sandberg, M.; Weber, S. G. *Biophys. J.* **2008**, *94*, 4561.

39. Chen, W. *Neuropharmacology* **2007**, 53(5), 664.

40. Bilkei-Gorzo, A. *Psychoneuroendocrinology* **2008**, 33(4), 425.

41. Lucas, L.R. *Brain Res.* **2007**, 1155, 108.

42. Lugo, J.N.; Wilson, M.A.; Kelly, S. J. *Neurotoxicol. Teratol.* **2006**, 28(2), 238.

43. Holt, A.G.; Newman, S.W. *Brain Res.* **2004**, 1030(1), 28.

44. Hui, K.-S.; Saito, M.; Hui, M. *J. Biol. Chem.* **1998**, 273(47), 31053

45. Hersh, L.B.; Aboukhair N.; Watson S. *Peptides***1987**, **8**(3), 523.

46. Raff, M.C. *Nature* **1978**, 274(5673), 813.

47. Hui, M. and Hui, K.-S. *Neurochem. Int.* **2008**, 53(6-8), 317.

48. Horsthemke, B.; Hamprecht, B.; Bauer, K. *Biochem. Biophys. Res. Commun.* **1983**, 115(2), 423.

49. Chen, J-G.; Woltman S. J.; Weber S.G. *J. Chromatogr. A* **1995**, 691, 301.

50. Brinkman U.A.; Frei R.W.; Lingeman H. *J. Chromatogr.* **1989**, 492, 251.

51. J.F.K. Huber, K.M. Jonker, H. Poppe, *Anal. Chem.***1980,** 52, 2.

52. P. Kucera, H. Umagat, *J. Chromatogr. A* **1983,** 255, 563.

53. W.F. Nirode, T.D. Staller, R.O. Cole, M.J. Sepaniak, *Anal. Chem.* **1998**, 70, 182.

54. Wu J.; Xu K.; Landers J.P.; Weber S.G. *Anal. C hem.* **2013**, In press.

Chapter 2 Electroosmotic Sampling. Application to Determination of Ectopeptidase Activity in Organotypic Hippocampal Slice Cultures.

This work has been published in *Anal. Chem.* **2010**, 78, 1761-1768.

2.1 Introduction

Neuropeptides play a key role in brain and peripheral nervous system functions such as pain and learning[1]. They are mainly inactivated by ectopeptidases – outward-facing, membrane-bound peptidases that cleave the active peptides into inactive fragments[2-4]. Extracellular peptidases create active forms of BDNF[5], substance P[6], cholecystokinins[4] and alter the activity of dynorphins[7]. Recent work shows that peptidases are important in the degradation of amyloid[8, 9]. Also, attenuated peptidase activity following stroke can contribute to neurotoxicity and an endogenous blocker of the ectopeptidase that cleaves enkephalin has powerful analgesic effects[10]. Thus, a deeper understanding of peptidase activity is necessary for understanding both normal and pathological brain function, as well as for the development of novel strategies for drug development.

While the central focus of this paper is electroosmotic sampling, the determination of peptidase activity *in tissue* is an important direction. Peptidase activity has been a concern in microdialysis experiments. Microdialysis sampling of peptides is improved in the presence of peptidase inhibitors[11-17]. Recently, the Stenken group[18, 19] has developed microdialysis approaches to *in vitro* (enzyme solutions) determination of protease activity. *In vitro* (slice) studies of peptidase inhibitors lead to knowledge of the peptidases active in a whole slice[15, 20]. Finally, several research groups have analyzed peptidase activity (dynorphin A[21, 22], substance P[23], endorphin[24], and peptide E[25]) *in vivo* with microdialysis. Most of our understanding of peptidases has come from analysis of tissue extracts, homogenate or fraction by determination of peptide fragments by HPLC[26, 27] or by standard enzyme methods (fluorogenic substrate)[28, 29]. More modern methods are demonstrating more chemically detailed information at the organism level. For example, high resolution separations followed by mass spectrometry have been used to

investigate a knockout mouse missing the gene producing dipeptidyl peptidase 4 allowing the discovery of the influence of that enzyme on the peptidome[30, 31]. In another example, mass spectrometry was applied to the analysis of the differential peptidome in rat striatum resulting from K^+-induced depolarization[32]. The approaches illustrated open the possibility of asking and answering more refined questions about peptides and peptidases, including localized measurements in tissue, *in vivo* and *in vitro*. One pragmatic issue concerning analysis of *ecto*peptidase activity is that any tissue fractionation will release intracellular peptidases that will contribute to peptide breakdown. It follows that it is preferable to perform analysis of ectopeptidase activity with intact cells or tissues when possible.

The organotypic culture method provides a route to *in vitro* models of *in vivo* tissue. Stoppini and co-workers described a simple preparation technique for hippocampal organotypic cultures[33]. The hippocampus is a brain area responsible for some forms of memory and learning, and is highly susceptible to damage from seizures, ischemia and anoxia[34]. Cultured hippocampal tissue survives for several weeks. The local synaptic circuitries are still functional and the structure of the hippocampus is well preserved[35]. In a wide spectrum of studies, the organotypic hippocampal slice culture (OHSC) has been established as a reliable model[2, 36]. For our purposes, OHSC-based assays allow for better control of the extracellular environment than is possible *in vivo*. Thus, for studying ectopeptidases, a medium free of soluble peptidases can be used[3]. Neuropeptide hydrolysis in the extracellular space in slice cultures has been reported[37] using the classical sampling approach in which tissue is incubated in a solution containing substrate, and products are detected in the medium after some time. Although this gives a measure of the endopeptidase activity in the entire slice, ectoenzyme activity in subregions of a specific brain area such as the hippocampus is not possible with this approach.

We propose a novel sampling method based on electroosmosis and apply it to OHSCs. The ζ-potential of OHSCs has been measured in our laboratory[38]. The ζ -potential is the potential of an object along a sh ear plane that separates fixed charges on the object and a moving electrolyte solution adjacent to it. In the OHSC, the fixed charges originate from charges on cells and the extracellular matrix. Application of an electric field to a porous medium like the OHSC with fixed charges creates an electroosmotic (EO) flow of the electrolyte. EO flow is the bulk fluid flow derived from the force of the electric field on mobile counterions that reside near the fixed charges. The magnitude of EO flow depends linearly and independently on the magnitudes of ζ-potential and the externally applied electric field. The OHSC's ζ-potential is -20 - -25 mV suggesting that when an electric field is applied to the tissue, an electroosmotic flow containing extracellular solutes will be generated in the extracellular space. In this work, we demonstrate the feasibility of this novel electroosmotic sampling approach for extracelluar fluid extraction. We have applied this method to the determination of ectopeptidase activity on Leu-enkephalin in the CA3 region of rat OHSCs with HPLC-EC.

2.2 Experimental Section

2.2.1 Solutions.

All chemicals used in the preparation of OHSCs were purchased from Sigma (St. Louis, MO). All aqueous solutions were prepared with purified water from a Millipore Synthesis A10 system (Millipore Corporation, Billerica, MA). Gey's balance salt solution (GBSS) was fortified with 2.7 mM $MgSO_4$ and 0.45 % D-(+)-glucose. Culture medium consisted of 50% basal medium

Eagle, 25% Earle's balanced salt solution, 23% horse serum, 25 U/mL penicillin streptomycin solution, 1 mM L-glutamine and 7.5 g/L D-(+)-glucose. Hepes buffered salt solution (HBSS) was composed of (mM): 143.4 NaCl, 5.0 HEPES, 5.4 KCl, 1.2 $MgSO_4$, 1.2 NaH_2PO_4, 2.0 $CaCl_2$, and 10 D-(+)-glucose. The pH was adjusted to 7.40 with 0.5 M NaOH before filtering (0.45 μm PTFE). HBSS was kept frozen until use.

Peptides, inhibitors and sources were as follows: YGGFL, GGFL, GGFM and thiorphan (Bachem Americas, Inc, Torrance, CA); 2-Guanidinoethylthio succinic acid (GEMSA), puromycin, captopril and bestatin (Sigma, St. Louis, MO); $^{D}Y^{D}AG^{D}F^{D}L$ was synthesized by Biomedical Research Support Facilities (BRSF) of University of Pittsburgh. All solutions were prepared in HBSS solution.

2.2.2 Preparation of OHSCs.

The procedures described here have been approved by the IACUC of the University of Pittsburgh. The preparation of OHSCs is slightly modified from the Stoppini culturing method[33]. After rats (7 days postnatal) were decapitated, the hippocampal area was removed and chopped into 400 μm slices by a McIlwain tissue chopper (The Mickle Laboratory Engineering Co. Ltd, UK). Slices were placed in ice-cold GBSS solution using a dissecting microscope (Fisher Scientific, Pittsburgh, PA), the individual slices were then transferred onto membrane inserts (0.4 μm-pore size culture plate insert, Millipore Corporation, Billerica, MA) in a 6-well plate (Millipore Corporation, Billerica, MA), The slices were cultured over culture medium in a humidified incubator (Thermo Electron Corporation, Asheville, NC) at 37 ºC with 5% CO_2/air. Medium was exchanged every three days. Slices were normally cultured for 6 to 8 days. Before use, medium was removed from the dishes and replaced with GBSS (refrigerated till use and

warm up to 37 ºC), incubated (37 ºC) for 30 minutes, the previous step was repeated, and then the OHSCs were kept in HBSS (37 ºC).

2.2.3 Cell Death Determination

An inverted fluorescent microscope (Olympus IX71) with an Olympus Plan Apo 1.25× objective lens (both from Olympus, Melville, NY) was employed to image the OHSCs using a CCD camera (ORCA-285 IEEE 1394 -Based Digital Camera, Hamamatsu Photonics K.K., Japan). A Semrock (Rochester, NY) DA/Fl/TA-3X-A Triple-band ‘‘Pinkel’’ filter set (exciter I, 387 nm; exciter II, 494 nm; exciter III, 575 nm; dichromatic mirror: 394–414 nm, 484–504 nm, 566–586 nm; emitter: 457, 530, 628 nm) was used for imaging of propidium iodide (PI)-stained OHSCs. Details of this procedure can be found in the companion paper[39]. Briefly, following a sampling experiment, OHSCs were provided with fresh medium containing PI (final concentration is about 12 μM). After 16 to 24 hours, images were taken for *% death* measurement. The % death measurement is based on the fluorescence intensity of the PI in the sampled area. One hundred% death represents PI fluorescence from an OHSC killed by exposure to liquid methanol until opaque; 0% control OHSCs were handled (medium exchange, moved from incubator to lab and back) as experimental OHSCs, but were not sampled (Equation 1).

$$\%\, death = \ (MI_s - MI_c)/(MI_k - MI_c) \qquad (1)$$

where *MI* represents mean fluorescence intensity of PI, *s* is the sampled OHSC, *c* is the 0% control OHSC, and *k* is the 100% dead OHSC.

2.2.4 Electroosmotic Sampling Set-up.

In the sampling set-up as displayed in Figure 2.1, we had: a) two Petri dishes containing the same volume of solution to avoid siphoning; b) an insert membrane to hold the OHSC; c) a sampling capillary with one tip positioned near the tissue surface and the other one dipped into buffer solution in the other dish; and d) two Pt electrodes connected to a power supply to complete the electric circuit. An electronic micromanipulator (Model TSX-1, Sutter Instrument Company, Novato, CA) was used to position the capillary tip. Once an electric field is applied, fluid is drawn into the sampling capillary by electroosmotic flow. Samples were ejected from the capillary using a 50 µL syringe containing 40 µL (sometimes 20 µL) 0.1% TFA. This represents approximately a 100 (50)-fold dilution. A further 2 – 37.5-fold dilution depending on t he concentration of peptide in the bath was made before injection into an HPLC-EC system for analysis. A 150 µm ID × 30 cm (length) capillary was used in all experiments unless described otherwise.

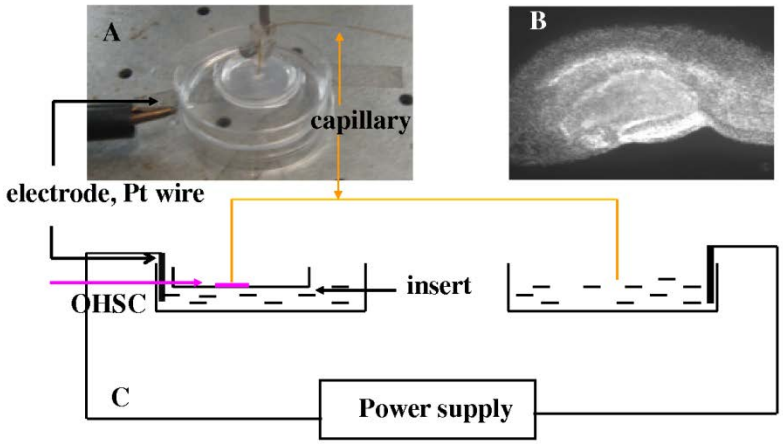

Figure 2.1 The set-up for electroosmotic sampling. A. a picture of the left side of the set-up B. a bright field image of an OHSC C. a schematic figure of the set-up.

2.2.5 HPLC-EC System.

We utilized a Waters 600 E quaternary pump (Waters Corporation, MA) to deliver the mobile phase (23% acetonitrile, 3% 1-propanol, 0.1% trifluoroacetic acid and Milli-Q water) at 100 µL/min and a simple tee to split the flow. After splitting, the mobile phase flowed through a VICI injector (Valco Instruments Co., Houston, TX) and then a 75 µm ID capillary column at about 1 µL/min. The 9-cm long column was packed with 2.6 µm C_{18} particles in the laboratory as described by Kennedy et al[40]. Peptides were detected electrochemically following a postcolumn reaction. The effluent from the column was mixed with biuret reagent (0.24 M carbonate buffer, 12.0 mM disodium tartrate and 2.0 mM copper sulfate, pH 9.83) to form electrochemically active complexes which were detected at a 10 µm carbon fiber electrode at an applied potential of +0.55 V versus Ag/AgCl. Potential was controlled with a BAS Epsilon potentiostat (W. Lafayette, IN). Biuret reagent was delivered by an Isco model DM syringe pump (Harvard Apparatus, Holliston, MA) at 0.3 µl/min. The post column derivatization was performed in a Capillary Taylor Reactor (CTR)[41] with an inner diameter of 75 µm. The HPLC-EC system was depicted by Xu et al.[42]. Under the specified conditions and with peptide concentrations less than 1 µM, this system gives baseline resolution for the peaks of interest. Peak height and peak area (PeakFit Version 4, AISN Software, Inc.) are proportional to concentration. Because we pack columns locally and we use flow splitting, there is a variability of retention times. Thus, peptide standards are always used for peak assignments.

2.2.6 Observation of Electroosmotic Flow in Tissue.

This experiment was carried out to create an image that would demonstrate the phenomenon – that the application of an electric field pulls solution through the tissue. Samples obtained from this experiment were not analyzed. An insert membrane supporting an OHSC was placed into a Petri dish (60 × 15 mm) containing approximately 3 mL of HBSS. A100 μm ID × 30 cm long fused-silica sampling capillary filled with HBSS was held orthogonal to and just touching the OHSC. The proximal end of the capillary was placed in a vial containing HBSS and a platinum wire (1 mm diameter). The vial was sealed and positioned to avoid siphoning. A gold minigrid electrode (~5 μm thick) was placed on the bottom of the Petri dish, under the insert membrane/OHSC. The platinum wire and gold minigrid were connected to a high voltage power supply (Stanford Research Systems, model PS350, Sunnyvale, CA). A slit was cut into the side of the Petri dish, allowing for a 25 μm ID fused-silica injection capillary to be positioned under the insert membrane and above the gold minigrid. Capillaries were cut flat and clean using a Shortix capillary cutter with a diamond blade (Middelburg, Netherlands). The injection capillary was filled with 10 μM Thioglo-1 (Covalent Associates, St. Louis, MO) in HBSS. The tissue and minigrid were in the optical path of the IX-71 inverted fluorescence microscope and imaged using a U Plan Apo 4× objective lens (Olympus) and a specially-built Omega fluorescence cube (Omega, Brattleboro, VT): 378 nm excitation and 480 nm emission. Simple PCI software acquired the images. When the tissue is in place, image acquisition was initiated. In experiments (controls) three (zero) kV were applied to the system, followed by the injection of Thioglo-1 dye under the insert membrane.

2.3 Result and Discussion

2.3.1Demonstration of Electroosmotic Sampling

2.3.1.1 Proof of Principle.

Initial proof of principle experiments were carried out by exposing tissue to a low concentration of a neutral, membrane permeant, thiol reactive, fluorogenic reagent, Thioglo-1. This reagent reacts with thiols in the cell, chiefly glutathione (GSH). Cells exposed to this reagent become fluorescent rapidly. In experiments, a blunt-ended, electrolyte-filled capillary was placed on the tissue. Contact with the tissue can be discerned while doing the capillary placement, however the image of the end of the capillary when it is in place is quite variable, as the image is taken through the minigrid, the support membrane, and the tissue. (See Figure 2.2: A1 and B1). A brief injection of the Thioglo-1-containing electrolyte under the insert membrane supporting the tissue leads to significant fluorescence under the capillary and in the capillary lumen in the experiment (B1-B3 in Figure 2.2). In the control where no electric field is applied, no change is observed in the image (A1-A3 in Figure 2.2). This demonstrates that application of an electric field through the OHSC and insert membrane into a fused-silica capillary creates an electroosmotic flow into the capillary lumen. Thus, the cells around the capillary opening fluoresce with Thioglo-1. Without the electric field, there is no change in the luminescence intensity near the sampling capillary.

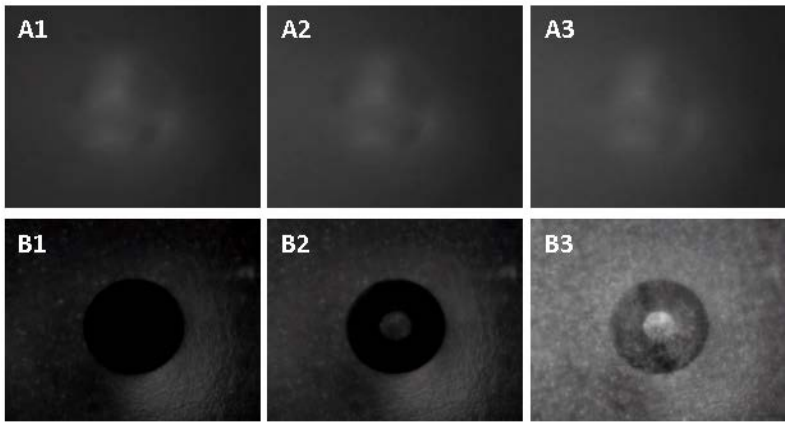

Figure 2.2 Inverted fluorescence image (4× objective lens) of an OHSC, grown on an insert membrane, with a fused silica capillary positioned orthogonally, directly above the OHSC. A. No applied voltage at time 1) 0 s, 2) 6.6 s, and 3) 13.2 s. B. 3 kV applied, images taken at times 1) 0 s, 2) 6.6 s, and 3) 13.2 s. The Thioglo-1 injection capillary is outside of the field of view of these capillaries.

2.3.1.2 Peptide Sampling.

YGGFL is a neutral neuroactive peptide. Its enzymatic hydrolysis was employed as a probe to evaluate electroosmotic sampling. We used $^{D}Y^{D}AG^{D}F^{D}L$, an analog of YGGFL containing D amino acids, as an internal standard (IS). This peptide is resistant to enzymatic degradation[43] . Solutions of the IS and YGGFL in HBSS comprise the medium during sampling. As described in the experimental section, an electrolyte-filled capillary is placed perpendicular to and near or touching the surface of an OHSC which is in contact with the medium through an insert membrane. When current flows from the medium beneath the OHSC into the capillary, electroosmotic flow will carry neutral molecules of similar size and shape into the capillary at about the same flow rate. Thus YGGFL and the IS will have very similar velocities since they

are both virtually neutral and they have similar molecular weights. The biuret complex of the IS also has a similar electrochemical response to the biuret complex of YGGFL. Thus, if the concentrations of the two species are the same in the bath, the YGGFL peak will have a similar area to the IS peak if there is no enzymatic degradation.

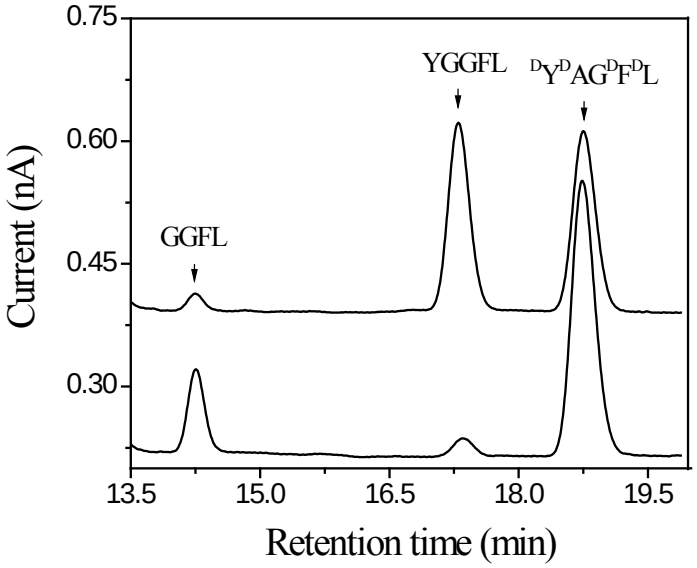

Figure 2.3 Demonstration of electroosmotic sampling. Chromatograms of samples obtained by 5 min electroosmotic sampling at an electric field of 46.7 V/cm with the capillary tip positioned on different surfaces: CA1 sub-region of an OHSC (bottom) and the surface of the same insert membrane adjacent to the OHSC (top). 150 μM YGGFL and $^{D}Y^{D}AG^{D}F^{D}L$ (IS) in HBSS buffer solution served as the solution under the insert membrane. The samples were mixed with 20 μL 0.1% TFA for the former case and 40 μL 0.1% TFA for the latter.

Figure 2.3 displays typical chromatograms of the samples obtained by electroosmotic sampling. GGFL elutes first, followed by YGGFL and then IS. When samples are drawn through the OHSC, some of YGGFL is hydrolyzed into GGFL. The sum of the YGGFL and GGFL

concentration is still smaller than that of the IS, implying the presence of other undetectable products. When the capillary tip was moved onto the insert membrane surface adjacent to the slice culture, the YGGFL peak is almost as large as the IS peak which means most of YGGFL remains intact during the sampling. Only a small GGFL peak is observed. The small GGFL peak results from the presence of cells in the membrane adjacent to the culture itself. The results clearly indicate that YGGFL has been carried through the slice culture and that it was hydrolyzed in the tissue. The result verifies the feasibility of this novel electroosmotic sampling method and implies its possible application in the enzymatic studies.

2.3.2 Damage Caused by Electroosmotic Sampling.

Figure 2.4 contains representative images of slice cultures taken before and after electroosmotic sampling compared with the image of a slice culture exposed to methanol. When the electrolyte-filled capillary tip was positioned directly on the surface of the slice culture, some cell death appears around the sampling area 18-24 h after sampling (a red area shows up in A2 compared with A1, the image taken from the same slice culture before electroosmotic sampling) but the rest of slice looks normal. When the capillary tip was placed 50 μm away from the surface of the slice culture (with electrolyte connecting them), no obvious damage occurs (no darker red is observed in B2 compared with B1). We report in more detail in a companion paper[39] that % death is less than 10% when sampling in CA3 for 5 min at an electric field of 46.7 V/cm, with a capillary having an inner diameter less than or equal to 180 μm, and positioned 15 μm or more from the surface.

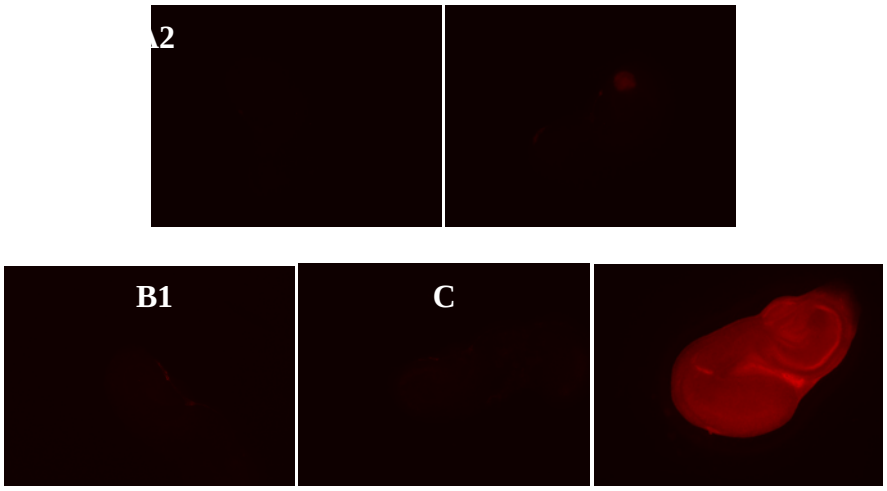

Figure 2.4 Images of OHSCs before (A1, B1) and after (A2, B2) 5 min sampling at an electric field of 46.7 V/cm with a 150 μm (ID) × 30 cm capillary. The capillary tip was positioned directly on (A2) or 50 μm away from theOHSC surface (B2). Image C is taken from a controlled OHSC treated with MeOH. Image A1 and A2 were taken from the same OHSC, as were B1 and B2.

The investigation of ectopeptidase activity should be immune to misinterpretation from damage. As membrane-bound proteins, their volume-average concentration does not change on the minutes timescale over which sampling occurs. They do not rely on metabolism to function. Indeed, most assays begin by homogenizing the tissue! Thus, our approach is quite gentle by comparison. This is not to say that the cell death and even the electric field itself may be unwanted in a particular experiment. Certainly, a level of caution must be used in applying any sampling procedure to live tissue.

The ζ-potential of a OHSC has been measured to be about -22 mV in our laboratory[38], while it is about -50 mV for a silica capillary after proper preconditioning. The mismatch in ζ-

potential produces a pressure driven flow into the capillary which forces the slice surface against the capillary tip during electroosmotic sampling. This may contribute to the physical damage when the capillary is actually touching the tissue. Joule heating at the capillary tip might be another source of the damage.

Table 2.1 The Possibility of Cytosolic Enzyme Release under Very Tough Conditions

Runs	1	2	3	4
Difference in conversion rates	-5%	2%	2%	-1%

p-value of a student t- test = 0.39

Electric field was 67.7 V/cm; capillary ID was 180 μm and the sampling time was extended to be 15 min.

To see whether the sampling process causes the release of cytosolic enzymes during electoosmotic sampling, we carried out the following experiments under conditions as given in Figure 2.4: samples were collected and split after sampling. One aliquot was mixed with 0.1% TFA (to stop enzyme activity) right after the sample was collected, whereas the other aliquot remained at room temperature for 45 min before 0.1% TFA was added. The conversion rates of GGFL from YGGFL, defined as *[GGFL]/([GGFL]+[YGGFL])*, were measured for both aliquots. The differences in conversion rates (shown in Table 2.1) were statistically zero (four repeats; % difference ranging from -5% to 2%, p = 0.38 for null hypothesis that there is no difference). Thus, YGGFL hydrolysis did not continue after the sample collection implying that no soluble cytosolic peptidases were extracted. Therefore, only the membrane-bound ectopeptidases hydrolyze YGGFL during electroosmotic sampling. This is an advantage in comparison to

procedures that homogenize tissue. Sampling the extracellular space excludes the influence from those membrane-bound enzymes having their active sites facing intracellularly.

2.3.3 Measurement of Sampling Flow Rate

2.3.3.1 Single IS Method.

During electroosmotic sampling, existing extracellular fluid reaches the sampling capillary before solution from the bath that is drawn through the OHSC. It is the latter solution that contains IS. Thus, the total sampled volume should be the sum of these two volumes as expressed below:

$$V_S = V_{ECF} + V_{BATH} \quad (2)$$

V_{ECF} and V_{BATH} represent the sampled volume from the extracellular space and the bath solution, respectively. V_{BATH} is obtained from sampled mol_{IS} (see equation 2 in Supporting Information) divided by the initial concentration of IS in the bath. V_S, the total sampled volume, is proportional to the applied electric field. By rearranging Eq. 2, we obtained

$$V_{BATH} = V_S - V_{ECF} = kEt - V_{ECF} \quad (3)$$

E is the applied electric field, t is the sampling time, and k is related to the 'apparent' ζ-potential (ζ_{APP}) in the tissue by

$$k = -(\varepsilon\zeta_{APP}/\eta)\pi \cdot a^2 \quad (4)$$

where a is capillary radius, ε is permittivity, and η is viscosity. We use 'apparent' ζ -potential to account for the ζ-potential mismatch between the capillary and the OHSC mentioned above. There will be a small contribution from pressure-induced flow adding to the electroosmotic flow. As we do not explicitly account for this in Eq. 4, we use an apparent ζ-potential. By plotting

V_{BATH} against E, we obtained V_{ECF} from the y intercept as 205 ± 55 nL. The sampling flow rate can be calculated as V_S divided by the sampling time. It ranges from 60 to 150 nL/min under the conditions applied. The apparent ζ- potential is about -29 mV slightly larger in magnitude than the measured ζ- potential of an OHSC, -22 ± 2 mV. The observed difference between the previously measured and the apparent ζ-potentials is consistent with the flow having a small pressure-induced component due to the larger (negative) ζ-potential in the capillary.

It is interesting to note that the applied field controls where the sample comes from. The linear regression of V_{BATH} on E (V_{BATH}= 10.3 E (V/cm) – 205 nL) shows that a field of 20 V/cm will provide a V_{BATH} of zero. Thus, fields below 20 V/cm provide extracellular fluid from the tissue under the conditions used, whereas fields greater than that will sample fluid from the bath below as well as the extracellular fluid. Consequently, conditions for obtaining the extracellular fluid, and thus capturing endogenous species, are easily attained.

2.3.3.2 Two IS Method.

In many experiments, an average flow rate based on the data just discussed may be sufficient. However, it would be beneficial in some circumstances to have an indication of the flow rate for each run. GGFM, used as a second internal standard, is filled in the sampling capillary. When sampling starts, GGFM solution is gradually replaced by extracellular fluid and then by bath solution. Thus, the sampling capillary is filled with GGFM solution, extracellular fluid and bath solution in the end if the sampling time is not too long. Eq. 5 expressed the volume distribution in the capillary.

$$V_{capillary} = V_{GGFM} + V_{ECF} + V_{BATH} = V_{GGFM} + V_S \quad (5)$$

In every run of sampling, both V_{GGFM} and V_{BATH} can be indirectly obtained from the chromatograms. $V_{capillary}$ is determined based on a chromatogram from the capillary filled with

GGFM solution only. V_S and V_{ECF} can be calculated according to Eq. 5. Thus, the two IS method allows a direct determination of sampling flow rate in every run. The average sampling flow rate, 112 ± 43 (s.d.) nL/min at an electric field of 50 V/cm, is indistinguishable from103 nL/min, obtained from the single IS method under the same conditions. The large standard deviation confirms the need for this two IS method. The sampling flow rate is easily adjusted by t he applied electric field and the diameter of the capillary.

2.3.4 Sampling Bias.

The observed mobility of a molecule in the extracellular space is the sum of its electroosmotic mobility and its electrophoretic mobility. For a negatively charged species whose electrophoretic mobility opposes its electroosmotic mobility, sampling could be a problem. According to Eq.6,

$$u_{OBS} = u_{CE} + u_{EO} = \frac{z}{6\pi\eta r} + \frac{\varepsilon\zeta}{\eta} \qquad (6)$$

where u_{OBS}, u_{CE} and u_{EO} represent the observed mobility, electrophoretic mobility and electroosmotic mobility, respectively. z is the net charge of the molecule, η is viscosity, r is the Stokes radius, ε is permittivity and ζ is zeta potential. For a low-molecular-weight species with a negative charge of - 0.6, the solute's velocity is 0 a s the electroosmotic and electrophoretic mobilities are equal and opposite. In practice, however, the pressure-driven flow generated by the ζ-potential mismatch works to minimize this problem. For example, fluorescein which is practically a dianion at physiological pH, can be sampled electroosmotically.

2.3.5 Indentifying the Peptidase Pharmacologically by Electroosmotic Sampling.

There are several peptidases that may act upon Leu-enkephalin in rat brain. The aminopeptidases (aminopeptidase N (APN), puromycin- sensitive aminopeptidase (PSA) and two neuron specific aminopeptidases (NAP and NAP2)) cleave the N-terminal tyrosine from enkephalins. Other enzymes include carboxypeptidase, angiotensin-converting enzyme (ACE), dipeptidyl aminopeptidase (DAP) and enkephalinase (NEP), which hydrolyze YGGFL at other amide bonds. This aminopeptidases can be separated into two categories: bestatin-sensitive aminopeptidase (APN) and puromycin-sensitive aminopeptidase (PSA, NAP and NAP2). Puromycin-sensitive aminopeptidases are effectively inhibited at 20 μM puromycin[44-46]. Carboxypeptidases cleave YGGFL at the Phe-Leu amide bond with a K_m in the mM range[47]. This enzyme is specifically inhibited by GEMSA. DAP cleaves YGGFL into YG and GFL. This peptidase is primarily located in the cytosol - its membrane activity is low[48]. NEP and ACE cleave YGGFL to produce YGG and FL[49]. Thiorphan is a selective inhibitor for NEP while captopril inhibits ACE. Based on this information, we used puromycin, thiorphan, GEMSA, captopril, and bestatin to selectively block particular classes of peptidases in order to determine which peptidase is the most important in YGGFL hydrolysis in OHSCs. Typical chromatograms are displayed in Figure 2-5. Note that high concentrations of YGGFL were used because of the high K_m values anticpated. An approximately 200 – 3700-fold dilution of the sample preceded analysis to keep the injected concentration less than 1 μM (see experimental section).

GGFM elutes at about 10.5 min, followed by GGFL, YGGFL and IS. Four experiments were performed under conditions described in Figure 2.5. A one-way analysis of variance of the enzyme rate based on either GGFL production or YGGFL loss (see SI for the derivation of enzyme rate) shows that a significant difference exists among experiments A, B, C, and D.

However, there is no significant difference among experiments A, B, and C. Thus, bestatin is the most effective inhibitor. We conclude that a bestatin-sensitive aminopeptidase may contribute in the inactivation of exogenous YGGFL in the extracellular space in the CA3 region of the hippocampus.

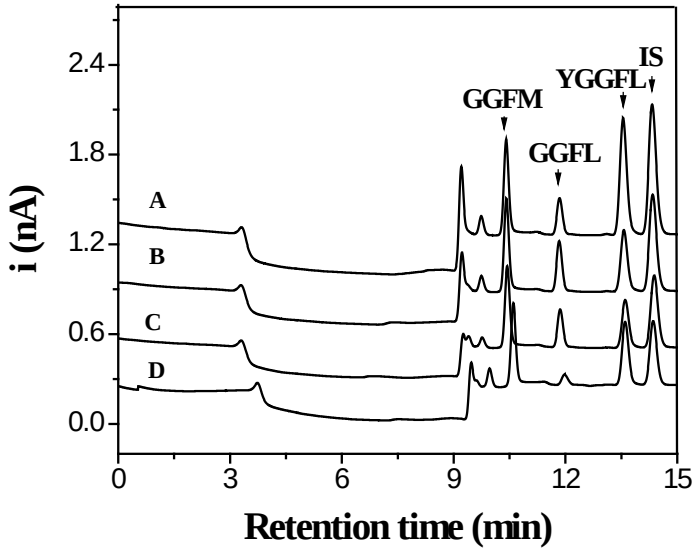

Figure 2.5 Five min sampling through CA3 at 50 V/cm. The bath solution is HBSS with 150 μM YGGFL and IS with or without inhibitors as follows: Experiment A, no inhibitors; B, includes inhibitors (μM) of thiorphan (15), GEMSA (210), captopril (25). C, As B plus puromycin (20). D, as C plus bestatin (100).

The degradation paths of YGGFL depend on the tissue being studied and the method of measuring enzyme activity. The cleavage of the Tyr-Gly amide bond represents the only detectable inactivation pathway in homogenates or soluble fractions of brain tissue, while cleavage of the Gly-Phe bond represents about 20% with particulate fractions[50] and may even reach 65% with synaptosomes[51]. In our observations in the OHSC, 72% of YGGFL hydrolysis

occurs at Tyr-Gly. The hydrolysis at Tyr-Gly of exogenous YGGFM in rat striatal slices is about 80% of the total hydrolysis[37], which is similar to our result. In this experiment, YGGFM diffuses into the entire extracellular space and reacts with the ectoenzymes. There is a considerable variation in enkephalin-degrading activity across the human brain[52]. This emphasizes the necessity of spatial resolution, something that the current approach can provide.

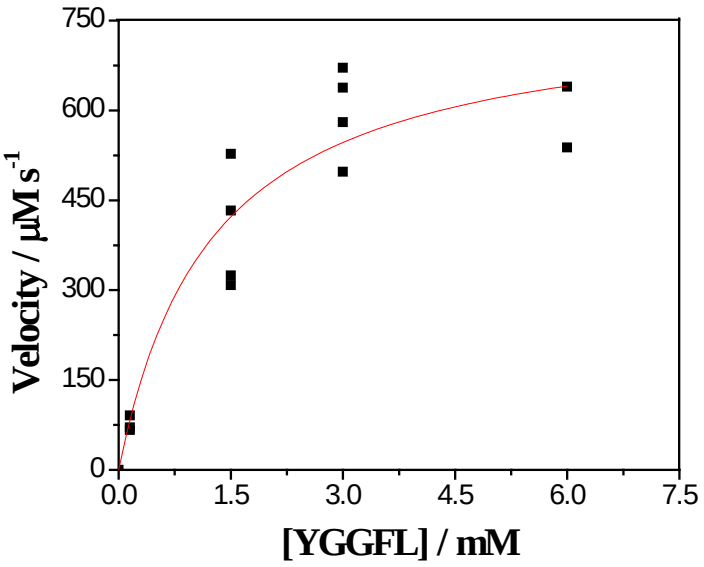

Figure 2.6 Substrate saturation curve for ectoaminopeptidase-catalyzed YGGFL hydrolysis. All bath contains 15 μM thiorphan, 210 μM GEMSA, 25 μM captopril and 20 μM puromycin.

Finally, we challenged OHSCs with different concentrations of YGGFL to determine a value of K_m. The initial velocity is defined as [GGFL]/t_e, where t_e is the exposure time of YGGFL in the OHSC (see Supplemental Information for details of t_e derivation) t_e is calculated to be 1.5 s under the conditions used. This calculation involves the assumption that the sampled volume is a cylinder in the tissue with the same diameter as the inside diameter of the sampling

capillary, which is probably an underestimate. The initial velocity is plotted (Figure 2.6) as a function of [YGGFL], the initial concentration of the substrate. The YGGFL hydrolysis displayed a typical Michaelis-Menten behavior. We obtained V_{max} and K_m as 770 ± 95 μM/s and 1.2 ± 0.5 mM, respectively. This K_m value is similar to published values. While endogenous peptide concentrations tend to be low, peptidase K_m values are rather high. The high K_m values are consistent with the modest selectivity that is typical of peptidases.

Electroosmotic sampling appears to be effective. We have not determined the spatial resolution here quantitatively, however it is well known that the electric field, and thus electroosmotic velocity, decreases steeply as a function of distance from the tip. Of course, the electroosmotic velocity also depends on the applied field. We estimate, based on the images of tissue damage (when it occurs) that the spatial resolution is on the order of several hundred micrometers. This will need to be established more rigorously in the future. This distance dependence is proportional to the inside diameter of the capillary While there are complexities caused by the inhomogeneous electric field in the tissue, the overall approach is simple and ideally suited to slices or sampling from the surface of an organ, for example. *In vivo* application can be envisioned with narrower or pulled capillaries. Peptidase chemistry, e.g., selectivity, is very well understood (see http://merops.sanger.ac.uk/). However, ectopeptidase activity in intact tissue with spatial resolution is not. Imaging approaches based on fluorescence-generating substrates can provide more detailed information, even at the single-cell level, about the presence of peptidases[53-55]. For answering questions about native substrate metabolism, its space- and time-dependence, analysis of the native peptide substrate and its hydrolysis products is essential. The ability to measure peptidase activity with chemical and spatial selectivity should improve our understanding of how this important class of enzymes controls extracellular

peptide activity. Electoosmotic sampling could find its application as well in extracellular endogenous peptide extraction and determination when combined with appropriate quantitative analytical approaches. An important question is the relationship between the extracellular concentration and the concentration in the sampled fluid. While this remains to be determined, we have good reason to believe that calibration in a suitable matrix, e.g., sampling from a well-characterized hydrogel with a known ζ-potential, will be possible.

Reference

1. Oegren, S. O.; Kuteeva, E.; Elvander-Tottie, E.; Hoekfelt, T. *Eur. J. Pharmacol.* **2009**, *626*, 9.
2. Kenny, A. J. *Peptidergic Neuron* **1996**, 87.
3. Konkoy, C. S.; Davis, T. P. *Trends Pharmacol. Sci.* **1996**, *17*, 288.
4. Roques, B. P. *Trends Pharmacol. Sci.* **2000**, *21*, 475.
5. Lee, R.; Kermani, P.; Teng, K. K.; Hempstead, B. L. *Science (Washington, DC, U. S.)* **2001**, *294*, 1945.
6. Karlsson, K.; Sharma, H.; Nyberg, F. *Biomed. Chromatogr.* **2006**, *20*, 77.
7. Taira, A.; Tanno, K.; Sakurada, T.; Tadano, T.; Kisara, K. *Annu. Rep. Tohoku Coll. Pharm.* **1996**, *43*, 139.
8. Liu, Y.; Studzinski, C.; Beckett, T.; Guan, H.; Hersh, M. A.; Murphy, M. P.; Klein, R.; Hersh, L. B. *Mol. Ther.* **2009**, *17*, 1381.
9. Thevenet, J.; Angelillo-Scherrer, A.; Price, M.; Hirt, L. *J. Neurochem.* **2009**, *111*, 828.

10. Wisner, A.; Dufour, E.; Messaoudi, M.; Nejdi, A.; Marcel, A.; Ungeeheuer, M.-N.; Rougeot, C. *Proc. Natl. Acad. Sci. U. S. A.* **2006**, *103*, 17979.

11. Charli, J. L.; Mendez, M.; Vargas, M. A.; Cisneros, M.; Assai, M.; Joseph-Bravo, P.; Wilk, S. *Neuropeptides* **1989**, *14*, 191.

12. Kajiro, T.; Nakajima, Y.; Fukushima, T.; Imai, K. *Anal. Chem.* **2002**, *74*, 4519.

13. Littlewood, G. M.; Iversen, L. L.; Turner, A. J. *Biochem. Soc. Trans.* **1987**, *15*, 894.

14. Mauborgne, A.; Bourgoin, S.; Benoliel, J. J.; Hirsch, M.; Berthier, J. L.; Hamon, M.; Cesselin, F. *J. Pharmacol. Exp. Ther.* **1987**, *243*, 674.

15. Rose, C.; Vargas, F.; Silhouette, B.; Devaux, B.; Schwartz, J. C. *Neuropeptides* **1995**, *28*, 157.

16. Williams, J. T.; Christie, M. J.; North, R. A.; Roques, B. P. *J. Pharmacol. Exp. Ther.* **1987**, *243*, 397.

17. You, Z. B.; Nylander, I.; Herrera-Marschitz, M.; O'Connor, W. T.; Goiny, M.; Terenius, L. *Neuroscience (Oxford)* **1994**, *63*, 415.

18. Steuerwald, A. J.; Villeneuve, J. D.; Sun, L.; Stenken, J. A. *J. Pharm. Biomed. Anal.* **2006**, *40*, 1041.

19. Wang, Y.; Zagorevski, D. V.; Stenken, J. A. *Anal. Chem.* **2008**, *80*, 2050.

20. Giros, B.; Gros, C.; Solhonne, B.; Schwartz, J. C. *Mol. Pharmacol.* **1986**, *29*, 281.

21. Klintenberg, R.; Andren, P. E. *J. Mass Spectrom.* **2005**, *40*, 261.

22. Reed, B.; Zhang, Y.; Chait, B. T.; Kreek, M. J. *J. Neurochem.* **2003**, *86*, 815.

23. Freed, A. L.; Cooper, J. D.; Davies, M. I.; Lunte, S. M. *J. Neurosci. Methods* **2001**, *109*, 23.

24. Reed, B.; Bidlack, J. M.; Chait, B. T.; Kreek, M. J. *J. Neuroendocrinol.* **2008**, *20*, 606.

25. Zhang, H.; Stoeckli, M.; Andren, P. E.; Caprioli, R. M. *J. Mass Spectrom.* **1999**, *34*, 377.

26. Ayyoub, M.; Monsarrat, B.; Mazarguil, H.; Gairin, J. E. *Rapid Commun. Mass Spectrom.* **1998**, *12*, 557.

27. Muller, S.; Ho, B.; Gambus, P.; Millard, W.; Hochhaus, G. *J. Pharm. Biomed. Anal.* **1997**, *16*, 101.

28. Bell Hannah, L.; Gooz, M. *Am. J. Med. Sci.* , *339*, 105.

29. Brama, P. A. J.; TeKoppele, J. M.; Beekman, B.; Van El, B.; Barneveld, A.; Van Weeren, P. R. *Ann. Rheum. Dis.* **2000**, *59*, 155.

30. Tagore, D. M.; Nolte, W. M.; Neveu, J. M.; Rangel, R.; Guzman-Rojas, L.; Pasqualini, R.; Arap, W.; Lane, W. S.; Saghatelian, A. *Nat. Chem. Biol.* **2009**, *5*, 23.

31. Tinoco, A. D.; Tagore, D. M.; Saghatelian, A. *J. Am. Chem. Soc.* , *132*, 3819.

32. Haskins, W. E.; Watson, C. J.; Cellar, N. A.; Powell, D. H.; Kennedy, R. T. *Anal. Chem.* **2004**, *76*, 5523.

33. Stoppini, L.; Buchs, P. A.; Muller, D. *J Neurosci Methods* **1991**, *37*, 173.

34. Holopainen, I. E. *Neurochem. Res.* **2005**, *30*, 1521.

35. Cho, S.; Wood, A.; Bowlby, M. R. *Curr. Neuropharmacol.* **2007**, *5*, 19.

36. Bausch, S. B. *Neuromethods* **2009**, *40*, 183.

37. De La Baume, S.; Yi, C. C.; Schwartz, J. C.; Chaillet, P.; Marcais-Collado, H.; Costentin, J. *Neuroscience* **1983**, *8*, 143.

38. Guy, Y.; Sandberg, M.; Weber, S. G. *Biophys. J.* **2008**, *94*, 4561.

39. Hamsher, A.; Xu, H. G., Y.; Sandberg, M.; Weber, S. G. *Anal. Chem* **2010**, 82, 6370.

40. Kennedy, R. T.; Jorgenson, J. W. *Anal. Chem.* **1989**, *61*, 1128.

41. Beisler Amy, T.; Sahlin, E.; Schaefer Kathleen, E.; Weber Stephen, G. *Anal. Chem.* **2004**, *76*, 639.

42. Xu, H.; Weber, S. G. *J. Chromatogr., A* **2009**, *1216*, 1346.

43. Wade, D.; Boman, A.; Waahlin, B.; Drain, C. M.; Andreu, D.; Boman, H. G.; Merrifield, R. B. *Proc. Natl. Acad. Sci. U. S. A.* **1990**, *87*, 4761.

44. Gros, C.; Giros, B.; Schwartz, J. C. *Biochemistry* **1985**, *24*, 2179.

45. Hui, K.-S.; Saito, M.; Hui, M. *J. Biol. Chem.* **1998**, *273*, 31053.

46. Hui, M.; Hui, K.-S. *Neurochem. Int.* **2008**, *53*, 317.

47. Schwartz, J. C. *Trends Neurosci.* **1983**, 15.

48. Horsthemke, B.; Hamprecht, B.; Bauer, K. *Biochem. Biophys. Res. Commun.* **1983**, *115*, 423.

49. Hersh, L. B. *Mol. Cell. Biochem.* **1982**, *47*, 35.

50. Schwartz, J. C.; Malfroy, B.; De la Baume, S. *Life Sci.* **1981**, *29*, 1715.

51. Vogel, Z.; Altstein, M. *Endog. Exog. Opiate Agonists Antagonists, Proc. Int. Narc. Res. Club Conf. :* **1980**, 353.

52. Mosnaim, A. D.; Nguyen, T. D.; Tse, R.; Puente, J.; Couceyro, P.; Wolf, M. E. *Neurochem. Res.* **2008**, *33*, 81.

53. Hobson, J. P.; Liu, S.; Leppla, S. H.; Bugge, T. H. *Methods Mol. Biol.* **2009**, *539*, 115.

54. Linder, K. E., *Application* pp 44.

55. Rajopadhye, M.; Groves, K.; Preda, D. V., (Visen Medical, Inc., USA). *Application*: **2009**, pp 121.

Chapter 3. Optimization of Postcolumn Reactor Radius in Capillary High Performance Liquid Chromatography. Effect of Chromatographic Column Diameter and Particle Diameter.

This work has been published on *J. Chromatogr. A* **2006**, 1113, 116-22.

3.1 Introduction

It is well-known that post-column reactions can improve sensitivity and selectivity in liquid chromatographic analysis[1-3]. In just the past couple of years, papers using postcolumn reactions for a variety of bioanalytical applications have appeared, including amino acids and peptides[4,5], for fatty acid hydroperoxides in MEKC[6], for japonicus/polysaccharide[7], for glucosylated flavonoids[8], for acetyl-CoA esters[9], for phosphorylated peptides[10], for drugs (competitive binding)[11], for glucose and insulin[12], for bradykinin[13], for drugs[14], for lipoproteins[15], for tocopherols[16], for phosphorylated sugars[17], for peptides[3, 18-21]. One should include the preparation of MALDI plates as a post-column reaction[22]. Recent applications in environmental chemistry using postcolumn reactors include glyphosate[23], iodate and bromate[24], thiourea[25], anions[26], and ion chromatography[27]. However, post-column reactors come with some disadvantages. The most obvious are the additional hardware and reagents required, and the band spreading associated with the additional mixing following the separation.

The band spreading issue, as it is treatable theoretically, has been addressed. Huber, Jonker, and Poppe[28] considered the problem of using rather slow chemical reactions following the separation. They concluded that a packed bed reactor was superior to an open tubular reactor. In their work they assumed that mixing, as opposed to reaction, was instantaneous. On the other hand, Kucera and Umagat[29] considered the case of post-column reactors for microbore columns. With smaller peak volumes than in 4.6 mm ID (inside diameter) columns, *microbore* columns pose more of a challenge for post-column reactor design. These workers considered a fast reaction, *o*-phthalaldehyde with amino acids and primary aliphatic amines. They proposed a simple tubular reactor. Special attention was paid to creating a low-volume mixing 'tee'. Peak variances depended linearly on the square of the reactor diameter, showing that the

chromatography was compromised. In other words, they did not employ a reactor diameter small enough to make the additional band spreading from the reactor negligible. With 50 cm x 1 mm columns operating at 35 μL per minute, and with an equivalent post-column reagent flow rate, they used postcolumn reactor tubing in the 180 to 250 μm ID range.

Other workers have optimized postcolumn reactors experimentally. The sheath-flow approach has proven suitable for CE of DNA[30]. Optimization of postcolumn conditions for chemiluminescence detection has been achieved[31]. Hollow fiber membrane systems have been optimized to minimize band spreading[32]. The virtue of inducing secondary flow for improving radial mixing has been shown by Selovaka et al.[33]. Contributions to band spreading were evaluated in a postcolumn reactor for photochemical reactions[34] and for saccharides[35]. Much of this work is dated, and applies to columns with typical dimensions of 4.6 mm ID, 10-20 cm long with 5 μm diameter particles.

Recently, our group has developed a mixer that is well-suited to mix reagents with effluent from a *capillary* column[1, 36, 37]. This mixer, in conjunction with a fused silica Capillary Taylor Reactor (a simple, open tube long enough to permit diffusional relaxation of radial concentration gradients[1, 37]), creates a very simple postcolumn reaction device that does not increase band spreading under the conditions used[1]. In this system, diffusion-controlled reactions occurred in times on the order of one second, in physical volumes on the order of 10 s of nL[1, 37]. Kinetically controlled reactions require longer reactors[37].

The magnitude of the inside diameter or radius of the post-column reactor is an important variable. It controls the reactor's contribution to band spreading; smaller reactor radii are preferred from this perspective. However, as the HPLC column defines the flow rate, the pressure in the post-column reactor (of constant length) increases in inverse proportion to the

fourth power of the radius. Thus, there is clearly an optimal value for reactor radius. This paper determines that optimum, and demonstrates its dependence on column diameter and particle diameter.

3.2 Assumptions and Limitations

In chromatographic theory, there are many variables. If the number of variables can be reduced, the essence of the theory is often made clearer. However, there is also a sacrifice in the breadth of applicability of the results from putting limitations on the system. Thus, it is important to state and discuss the limiting nature of the assumptions.

We will set the value of three significant parameters by allowing them to depend on other freely chosen variables. One is the chromatographic velocity. We have set the velocity equal to the optimum velocity. Kennedy and Jorgenson[38] have shown that the optimum velocity in capillary columns is a function of the column diameter. In this paper, we have not taken that subtlety into account. Further, there are several formulations of H vs. v curves[39]. We have chosen to use the van Deemter equation (the expression is shown later), which works acceptably near the optimum velocity. Another parameter that is set is the post-column reactor length. Both theory[40] and experiment[1, 37] show that if the reaction is fast enough, it will be completed in a length of cylindrical tubing that depends upon the reagents' diffusion coefficients, the tubing radius and the velocity. Furthermore, the velocity in the reactor depends on the chromatographic velocity (which we fix) and geometrical parameters. Finally, we have taken the k' (the retention factor) of a solute to be zero.

The limitations that accompany these decisions are as follows. Setting the velocity at the optimum means that the analysis will favor total number of theoretical plates over theoretical plates per unit time. We analyze both in this paper. Setting the length of the post-column reactor means that the detector will give a 'full signal' for fast enough reactions, but not for kinetically slow reactions. Finally, the restriction on k' will make the reactor's relative (to the column) contribution to band spreading larger than it would be for a retained solute. A retained solute has a k'-dependent variance (time units). By using k'=0 in the formulations, we ignore this. The result is that the chromatography seems more sensitive to the presence of extracolumn band spreading than it would be for k'>0.

Finally, we assume that the chromatographic system operates at the maximum pressure of the pumping system. The ultimate limitation to chromatographic throughput is pressure[41]. As the velocity is fixed at the optimum, we control the length of the chromatographic column to use the available pressure.

In this paper, we determine how the system dimensions influence chromatographic performance as judged by the number of theoretical plates, N, and the number of theoretical plates per time. The results will show that there is an optimum in reactor radius that is dependent on the particle packing diameter and the column radius. Very small reactor radii lead to excessive pressure in the reactor, diminishing chromatographic performance by forcing a shortening of the column (remember, total pressure is fixed). Very large reactor radii lead to excessive band spreading in the reactor.

3.3 Equation Derivation

3.3.1 Reactor Requires Pressure

The total pressure in the system is given by Eq. (1).

$$P_m = \frac{\phi \eta v_c L_c}{d_p^2} + \frac{8 \eta v_r L_r}{a_r^2} \quad (1)$$

Here, P_m is the maximum pressure of the HPLC pump, η is the viscosity of the mobile phase, L_c and L_r represent the length of the column and the reactor respectively, v_c and v_r are the average linear velocities in the column and the reactor, respectively, d_p is the diameter of the packing particles, a_r is the radius of the capillary used to make the reactor, and ϕ is the column's permeability. The left-hand term on the right side is the pressure drop in the column[41] while the right-hand term is the pressure drop in the reactor. We will now use the assumptions described above with the van Deemter equation to remove some of the variables.

3.3.2 Average Velocity Is the Optimum Velocity.

$$H_c = \frac{2D}{v} + \lambda d_p + \frac{d_p^2}{gD} v \quad (2)$$

In the van Deemter equation, Eq. 2, H_c is the height equivalent to a theoretical plate for the chromatographic column, D is the solute's diffusion coefficient in the mobile phase, v is the average mobile phase velocity, d_p is the packing particle diameter, and λ and g are numerical, geometry-dependent constants (values of such parameters are discussed below). We choose the optimal velocity as the column velocity.

$$v_c = v_{opt} = \sqrt{2g}\,\frac{D}{d_p} \tag{3}$$

v_r is a function of v_c and the ratio of a_c, the radius of the column and a_r. The factor b in Eq. 4 below is equal to $\varepsilon_e + (1-\varepsilon_e)\varepsilon_i$, where ε_e is extraparticle porosity and ε_i is the intraparticle porosity.

$$v_r = v_c b(\frac{a_c}{a_r})^2 \tag{4}$$

3.3.3 Reactor Length Is the Length Required for Significant Diffusional Mixing.

L_r, the length of the reactor, is given by Eq. (5)[1, 37, 40]. We fix L_r based on capillary Taylor theory[1, 37]. The numerical factor represents the degree of mixing by diffusion. A larger number means more complete mixing. We choose 2.5 here, which means the length of the reactor is just enough for complete mixing. Kinetic factors are not considered here, thus extent of mixing is equivalent to the extent of reaction.

$$L_r = \frac{2.5 v_r a_r^2}{D} \tag{5}$$

3.3.4 Revised Pressure Expression

After substituting Eq. (3), (4) and (5) into Eq. (1), we obtain Eq. (6):

$$P_m = \frac{\sqrt{2g}\phi D \eta L_c}{d_p^3} + \frac{40 g D \eta b^2 (\frac{a_c}{a_r})^4}{d_p{}^2} \tag{6}$$

The first term on the right hand side of Eq. (6) is still the pressure drop across the column (P_c) while the second term is that across the post column reactor (P_r). This equation can be recast into a dimensionless ratio of column pressure to available pressure to give Eq. (7). In Eq. (7), the dimensionless second term of the right hand side is the fraction of the available pressure needed by the reactor.

$$\frac{P_c}{P_m} = \frac{P_m - P_r}{P_m} = 1 - \frac{40 g D \eta b^2 (a_c / a_r)^4}{d_p^2 P_m} \tag{7}$$

3.3.5 Reactor Adds Band Broadening.

Band spreading occurs in the reactor, but it may not be significant if the chromatographic peaks are broad. Thus, we must compare the extent of broadening from both sources. We have already shown experimentally that the mixer portion of the mixer/reactor adds no measurable broadening[1]. The variance (in units of time squared) for the column (at the optimum velocity) is given by Eq. (8).

$$\sigma_c^2 = \frac{H_c L_c}{v_c^2} \tag{8}$$

To get an expression for the variance, we will use the column length defined by pressure conservation (Eq. 9, from Eq. 6),

$$L_c = \frac{P_m d_p^3}{\sqrt{2g}\phi D \eta} - \frac{20\sqrt{2g} b^2 (a_c / a_r)^4 d_p}{\phi} \tag{9}$$

theoptimal velocity (Eq. 3) and the minimum value of H_c (H_{min}, Eq. 10) derived from the optimum velocity and the van Deemter equation (Eq. 2).

$$H_c = H_{\min} = (2\sqrt{\frac{2}{g}} + \lambda)d_p \tag{10}$$

After substituting Eqs. 3, 9 and 10 into Eq. 8, we get the final description for the column variance.

$$\sigma_c^2 = \frac{2\sqrt{\frac{2}{g}} + \lambda}{(2g)^{3/2} D^3 \phi \eta} d_p^6 P_m - \frac{20(2\sqrt{\frac{2}{g}} + \lambda)b^2}{\sqrt{2g} D^2 \phi} (\frac{a_c}{a_r})^4 d_p^4 \tag{11}$$

3.3.6 Variance in the Reactor

The variance in the same units for the reactor is given by Eq. (12)[1].

$$\sigma_r^2 = \frac{H_r L_r}{v_r^2} = \frac{v_r a_r^2}{24D} \frac{2.5 v_r a_r^2}{D} \frac{1}{v_r^2} = \frac{2.5 a_r^4}{24D^2} \tag{12}$$

L_r is defined above, and H_r is the height equivalent to a theoretical plate in a reactor[1],

$$H_r = v_r a_r^2 / 24D \tag{13}$$

3.3.7 Total Peak Variance

The total peak variance is the sum of the column and reactor variances.

$$\sigma^2 = \sigma_c^2 + \sigma_r^2 = \frac{2\sqrt{\frac{2}{g}} + \lambda}{(2g)^{3/2} D^3 \phi \eta} d_p^6 P_c + \frac{2.5}{24D^2} a_r^4 \tag{14}$$
$$= \frac{M}{D^3 \eta} d_p^6 P_m - \frac{40 g M b^2}{D^2} (\frac{a_c}{a_r})^4 d_p^4 + \frac{2.5}{24D^2} a_r^4$$

Here, we define M as $\frac{2\sqrt{2/g} + \lambda}{(2g)^{3/2} \phi}$.

The band broadening arising from the reactor can be considered negligible when it contributes no more than 10% extra to the peak width in the absence of the reactor. This is the case if $\sigma_r^2 / \sigma_c^2 \leq 0.21$.

3.3.8 Column Efficiency

N is defined here as the number of theoretical plates from the column when using an ideal reactor that requires pressure but adds no band spreading. The column variance, Eq. (11), is used to generate Eq. (15). *M* is defined above.

$$N = t_{0c}^2 / \sigma_c^2 = L_c / H_c = \frac{P_m d_p^2}{4g^2\phi^2\eta DM} - \frac{10b^2(a_c / a_r)^4}{\phi^2 Mg} \qquad (15)$$

However, with a postcolumn reactor, the retention time and the peak variance depend on more than just the column. The observed number of plates, N_{obs}, includes all effects of the reactor.

$$N_{obs} = \frac{t_0^2}{\sigma^2} = \frac{(t_{0c} + t_{0r})^2}{\sigma_c^2 + \sigma_r^2} = \frac{[Jd_p^2 + 5\phi(a_r / d_p)^2 - 40b^2(a_c / a_r)^4]^2}{4gMJ\phi^2 d_p^2 - 160gM\phi^2 b^2(a_c / a_r)^4 + 0.4\phi^2(a_r / d_p)^4} \qquad (16)$$

where, t_{0c} and t_{0r} are the dead time in the column and the reactor, respectively; *M* has the same definition as in Eq. (14); *J* represents the ratio $P_m / gD\eta$.

Eq. (16) looks unwieldy. However, N_{obs} is only dependent on P_m and three size-related variables, d_p, a_c and a_r. The figures based on these equations are much clearer. First, we will show the effect of column radius on the reactor choice. Secondly, we will find the relationship between N_{obs} and the variables d_p and a_r to get the optimal reactor radius for P_m equal to 4000 psi and a_c equal to 50 μm. Finally, the effects of P_m on the reactor choice will be shown.

To display the effect of the reactor, we also calculate the number of theoretical plates of the column under the same conditions but without the reactor (N_0) as below. Here, the pressure available for the column is the maximum offered by the pump.

$$N_0 = \frac{P_m d_p^2}{\phi \eta D(4 + \lambda\sqrt{2g})} \tag{17}$$

3.3.9 Description of Some Empirical Parameters

There are many parameters in this calculation procedure. Here, we list the parameters and discuss their origin and value: the column's permeability depends upon the method of packing and the particles for a packed column. For various columns, it ranges from 500 to 1000 [41]. We routinely obtain a value of 750 for 2.6 ~ 5 μm particle packings in 100 μm diameter columns. The effect of changes in ϕ on the results are negligible. λ and g are numerical, geometry-dependent constants. Typically, λ is 2 and g is 30 [39]. The value 2 comes from experiment and the simple random walk approach to eddy dispersion. The number 30 comes from assuming that the C term is governed by diffusional relaxation within the spherical particle. The value for λ will never be far from 2. The value for g would give a C-term in the Knox equation of 0.033, which is close to the observed value from many systems of C ~ 0.05. D is the diffusion coefficient of the solute in the mobile phase. η is the viscosity of the mobile phase. In our final expressions of N_{obs}, N and N_0, D and η always appear as the product Dη for a given solute and at constant temperature, this product, sometimes called the Walden product ($D\eta = RT / 6\pi a$ where R is the gas contstant, T is the temperature, and a is the radius of the diffusing molecule), will remain fairly constant as the solvent changes. We used 5.0×10^{-10} m^2/s as D and 0.001 $N\cdot s/m^2$ as

η. These values are typical for solutes of a few hundred Daltons molar mass and aqueous eluents. As the Walden product is in the final expressions, the product of these values is suitable for other solvents (but not dramatically larger or smaller solutes). b is equal to $\varepsilon_e + (1-\varepsilon_e)\varepsilon_i$, where ε_e is extraparticle porosity and ε_i is the intraparticle porosity. Usually, both porosities are near 0.4 [39], so b is 0.64. This term is appropriate if the mean, not the extraparticle, velocity is used in the van Deemter equation. Of all of the parameters, the value of g is the most dependent on the particular system (particle shape, intra- vs. interparticle mass transport limitation, diffusional vs kinetic stationary phase mass transfer limitation).

3.4 Results and Discussion

3.4.1 Effect of Column Diameter: Is a Capillary Taylor Reactor Useful for Large Columns?

The introduction discussed cases in which the simple Capillary Taylor Reactor added measurable band spreading with 4.6 and 1 mm ID columns. Table 3.1 provides a view of this problem. Table 3.1 shows the effect of a Capillary Taylor Reactor on the maximum number of observed theoretical plates, *Max* N_{obs}, as a function of d_p and a_c (Eq. 16). Values for N_0, the number of theoretical plates generated by the capillary column without the reactor (Eq. 17), are also given. The 'a_r range' is the range of reactor radii at which N_{obs} is at least 90% of N_0. The reactor can have a significant deleterious effect on the column efficiency. For a column having a radius of 150 μm, the *Max* N_{obs}/N_0 ratio increases from 19.5% to 99.9% as the diameter of packing particles increases from 1 μm to 5 μm. The influence of the reactor is small for the 2~5 μm particles but significant for 1 μm particles. The larger the column diameter is, the more effect the

reactor has on the column efficiency. The *Max* N_{obs}/N_0 ratio decreases as column radius increases. The a_r range in which N_{obs}/N_0 is larger than 90% becomes narrow or even disappears as column radius increases. Therefore, a small column is preferred when used with a Capillary Taylor Reactor especially when the column is packed with small particles. Specifically, the effect of the reactor is negligible when column radius is smaller than 150 μm for particle diameters greater than or equal to 2 μm.

Table 3.1 Effect of the column radius on N_{obs}/N_0. P_m=4000 psi; D=5.0×10^{-10} m^2/s; η=0.001 N·s/m^2; b=0.64; φ=750; g=30; λ=2.

d_p (μm)		1	2	3	4	5
N_0		3770	15100	34000	60400	94300
a_c = 150 μm	*Max* N_{obs}	735	13600	33400	60100	94200
	a_r range (μm)	-----	12	9-25	8-38	7-52
	Max N_{obs}/N_0	19.5%	90.1%	98.2%	99.5%	99.9%
a_c = 500 μm	*Max* N_{obs}	94	3600	25700	55600	91400
	a_r range (μm)	-----	-----	-----	26-35	22-52
	Max N_{obs}/N_0)	2.5%	23.8%	75.6%	92.1%	96.9%
a_c =1000 μm	*Max* N_{obs}	68	535	10000	41600	82000
	a_r range (μm)	-----	-----	------	-----	------
	Max N_{obs}/N_0	1.8%	3.5%	29.5%	68.9%	86.6%

3.4.2 Optimization of the Reactor Radius for Capillary Columns with Various Particle Sizes.

Figure 3.1 gives the relationship between the number of theoretical plates (N or N_{obs}) and the radius of the reactor a_r for a 100 μm ID column (a_c = 50 μm). N is the number of theoretical plates observed with a hypothetical reactor that requires pressure but causes no extracolumn band spreading. N_{obs} is defined by Eq. (16). N and N_{obs} depend similarly on a_r at small values of a_r. N and N_{obs} sharply increase and then reach a plateau or maximum as a_r increases. Larger particles exhibit a significant plateau, while the smallest particle size, 1 μm, shows a maximum. As a_r increases beyond the maximum, N does not change at all while N_{obs} gradually decreases. The shape of Figure 3.1 can be understood qualitatively by considering system for large and small values of a_r.

There is a minimum value of a_r that can be derived from Eq. 7. As a_r approaches $(40gD\eta b^2/(d_p^2 P_m))^{1/4} a_c$, more pressure is used to push fluid through the reactor. The column's length approaches zero, so N_{obs} approaches zero as well. Thus, the effect of the reactor on the column efficiency as a_r/a_c approaches $(40gD\eta b^2/(d_p^2 P_m))^{1/4}$ mostly comes from the pressure it steals. The pressure available to the column is increased with a larger diameter reactor, according to Eq. (7). For a large enough value of a_r, it will approach P_m. However, when a_r becomes large, the variance from the reactor becomes significant and cannot be neglected compared to the variance caused by the column. N_{obs} gradually decreases as a_r increases as shown on the right hand side of Figure 3.1 because of the effect of the reactor variance (Eq. (12)).

Obviously, what we are most interested in is the middle part of Figure 3.1 where the effect from the reactor is minimal and N_{obs} is the largest. Columns with larger packing particles

have a larger column variance, so there is a wider region of conditions that allow the band broadening from the reactor to be negligible compared to that from the column. Therefore, columns with larger packing particles have a wider plateau.

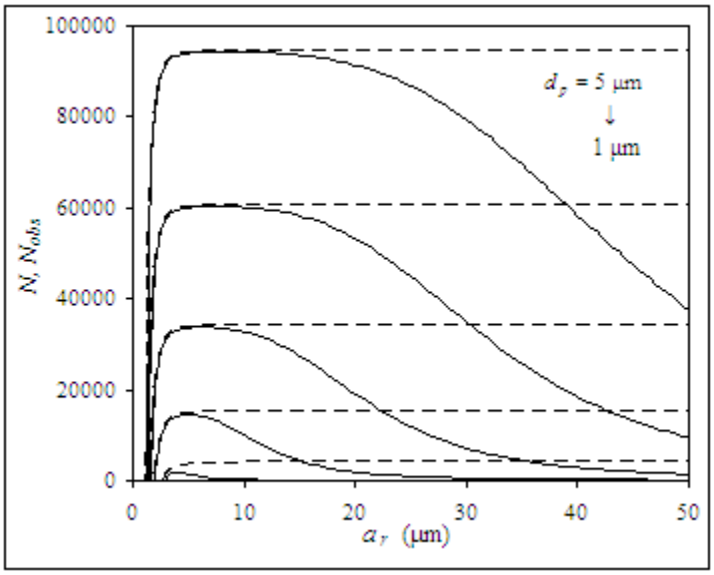

Figure 3.1 Plot of N (dashed line) and N_{obs} (solid line) against the radius of reactor. Each curve corresponds to a different particle diameter. The highest curve is for d_p = 5 μm, and the lowest is for d_p = 1 μm. a_c=50 μm; P_m=4000 psi; D=5.0×10^{-10} m^2/s; η=0.001 N·s/m^2; b=0.64;φ=750; g=30, λ=2.

Table 3.2 lists the range of reactor radii that give a value of N_{obs} that is larger than 90% of N_0, which we used to define the acceptable region. The parameters '*Max* N_{obs}', 'a_r range' and N_0 have the same definitions as in Table 3.1. t_0 is the retention time of an unretained solute. In addition, to determine whether it is possible to use a postcolumn reactor without significant sacrifice, Table 3.2 also compares *Max* N_{obs} with N_0. Values of *Max* N_{obs} for particle sizes from 2

to 5 μm are all larger than 90% of N_0. This is not the case with a 1 μm column, where *Max* N_{obs} is only 86.2% of N_0. This means that there is no reactor size that will yield an observed number of theoretical plates greater than or equal to 90% of N_0. The variance from a 1 μm column is quite small and the variance from the reactor is never negligible.

Table 3.2 Range of useful reactor radii with maximum N_{obs} as a criterion. a_c=50 μm; Other conditions are the same as in Table 3.1.

d_p (μm)	*Max* N_{obs}	a_r range (μm)	N_0	*Max* N_{obs}/ N_0	t_0 (s)
1	3250	-------	3770	86.2%	2.4
2	15000	4~14	15100	99.3%	39
3	34000	3~25	34000	100%	199
4	60400	3~38	60400	100%	628
5	94400	3~53	94400	100%	1533

Large values of N are often accompanied by long experimental time which is also shown in Table 3.2. To get a different perspective, we also looked at N_{obs} per unit time (N_{obs}/t_0) (Figure 3.2). Figure 3.2 displays how N_{obs}/t_0 changes with a_r. From Figure 3.2, with a proper size reactor, the N_{obs}/t_0 of a column with 1 μm particles can be more than four times larger than that of a 2 μm column, and over twenty times greater than a 5 μm column. Therefore, smaller particles are better in faster separations, even with a postcolumn reactor.

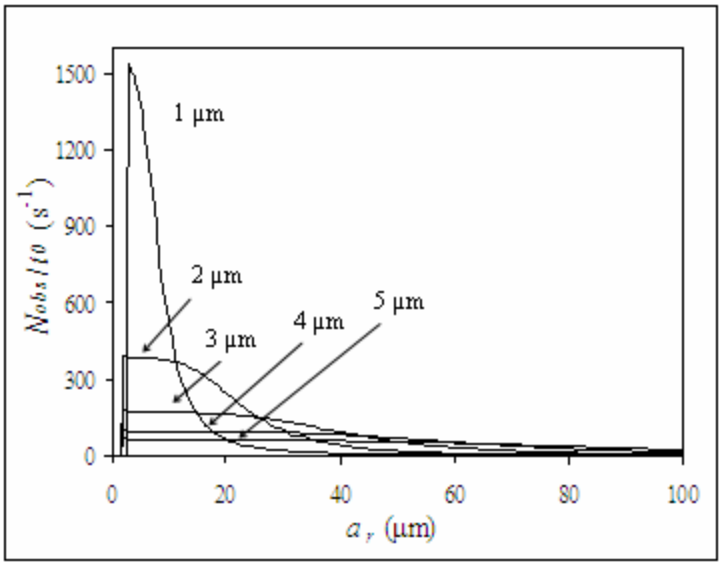

Figure 3.2 N_{obs}/t_0 (s^{-1}) as a function of a_r. Conditions are the same as in Figure 3.1.

Figure 3.2 is analogous to Table 3.2, but for the number of observed plates per time. It displays the range of a_r that will yield N_{obs}/t_0 that is at least 90% of N_0/t_0. Note that the range is only slightly different from that for N_{obs}. Similar to Table 3.2, columns with large particles have a wider plateau for N_{obs}/t_0.

3.4.3 The Special Case of 1 µm Particles: Is a Smaller Column Better When Using a Reactor?

As mentioned before, the reactor always affects the observed chromatographic efficency when d_p is 1 µm (as shown in Figure 3.1, there is no plateau there at d_p=1µm and Table 3.2, N_{obs}/N_0 always smaller than 90%). This is because the column variance from a 1 µm column is extremely small so that the variance from the reactor cannot be neglected. The only way to minimize the variance from the reactor is to use small radius reactors, which will be accompanied by a

sacrifice in available column pressure. However, Eq. (7) tells us that the pressure drop for the column will not change if a_c/a_r and d_p are constant. Therefore, for a given particle diameter, if the column diameter is scaled down as the reactor diameter is scaled down, the fraction of the maximum pressure available for the column should remain constant. That means when the column diameter is reduced, the reactor diameter should be reduced proportionally. Therefore, using a smaller column diameter might be helpful.

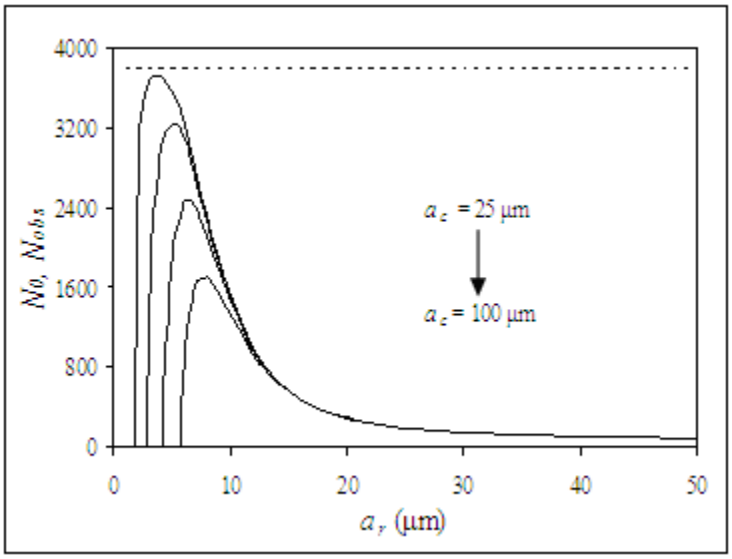

Figure 3.3. Plot of N_{obs} against the diameter of the post-column reactor. d_p=1 μm; a_c is altered from 25 to100 μm. The solid line represents N_{obs} while the dashed line represents N_0. Other conditions are the same as in Figure 3.1.

Figure 3.3 shows curves of N_{obs} for 1 μm particle packing plotted against reactor radius with column radius as a parameter. In Figure 3.3, the curves of N_{obs} vs. reactor radius increase sharply, reach a maximum and then gradually decrease at larger reactor radii. The maximum value of N_{obs} increases more than two times and the optimum value of a_r becomes smaller as the

column diameter changes from 100 μm to 25 μm. When the column radius is equal to or less than 42.5 μm, the *Max* N_{obs}/N_0 ratio starts to approach 90%, which means the reactor's effect is negligible at the optimal radius of the reactor, which is 5 μm.

3.4.4 Maximum Pressure (P_m) and Optimal Reactor Radius.

Results shown in Table 3-4 indicate the effect of P_m. *Max* N_{obs}, the maximum value of N_{obs} under optimal conditions, increases almost proportionally as P_m *i*ncreases. The 'a_r range' increases slightly as P_m increases. However, a_r, the reactor radius at which the maximal N_{obs} is achieved, is independent of P_m.

Table 3.3 Effect of the P_m on the acceptable range of reactor radii when a_c=50 μm. Other conditions are the same as in Table 3.1.

d_p (μm)		1	2	3	4	5
P_m=2000 psi	*Max* N_{obs}	1400	7500	17000	30200	47200
	a_r (μm)	5	7	10	12	14,15
	a_r range (μm)	-----	5-12	4-22	3-32	3-45
P_m =4000 psi	*Max* N_{obs}	3250	15000	34000	60400	94400
	a_r (μm)	5	7	10	12	14,15
	a_r range (μm)	-----	4-14	3-25	3-38	3-53
P_m= 8000 psi	*Max* N_{obs}	7000	30100	67900	121000	189000
	a_r (μm)	5	7	10	12	14,15
	a_r range (μm)	5	3-16	3-29	3-44	2-61

3.5 Conclusion

In this paper, the influence of the diameter of a Capillary Taylor Reactor on the performance of capillary liquid chromatography was studied. The reactor steals pressure from the column which in turn decreases the numbers of theoretical plates when small reactor diameters are used. At the same time, it adds some band broadening. The choice of the reactor radius actually depends on several factors such as packing particle size, maximal available pressure and column diameter. For packing particles larger than or equal to 2 μm, the Capillary Taylor Reactor is suitable for columns with radii not larger than 150 μm (For "suitable", we defined as if $N_{obs}/N_0 > 90\%$). A reactor with about a 12 μm radius (i.e., the commercially available 25 μm ID capillary) works well under such conditions. For 1 μm particles, however, the requirements are more stringent. Only columns with smaller than 42.5 μm radii can be used and the optimal reactor radius is 5 μm, which is much smaller compared to those coupled with larger particle packing columns. The results above are obtained under a maximal pressure of 4000 psi. The limitations in the column diameter become less restricted when a higher maximum pressure is available.

Reference

1. Beisler, A.T.; E. Sahlin, K.E. Schaefer, S.G. Weber, *Anal. Chem.* **2004**, 76, 639.
2. Brinkma, U.A.T., *Chromatographia* **1987**, 24, 190.

3. Freeman, M.K.; Daunert, S.; Bachas, L.G., *LC-GC* **1992**, 10, 112.

4. Ye, M.; Hu, S.; Quigley, W.W.C.; Dovichi, N.J., *J. Chromatogr. A* **2004**, 1022, 201.

5. Herraiz, T.; Casal, V.; Polo, M.C.; Lebensm, Z., *Unters. Forsch*. **1994**, 199, 265.

6. Schmitz, O.; Melchior, D.; Schuhmann, W.; Gab S., *J. Chromatogr. A* **1998**, 814, 261.

7. Lin , X.; Xu, D.S.; Feng, Y.; Shen, L., *Anal. Biochem*, **2005**, 342, 179.

8. Davis, B.D.; Brodbelt, J.S., *Anal. Chem.* **2005**, 77, 1883.

9. Shimazu, M.; Vetcher, L.; Galazzo, J.L.; Licari, P.; Santi, D.V., *Anal. Biochem*. **2004**, 328, 51.

10. Krabbe, J.G.; Lingeman, H.; Niessen, W.M.A.; Irth, H., *Anal. Chem.* **2003**, 75, 6853.

11. Schenk, T.; Molendijk, A.; Irth, H.; Tjaden, U.R.; Van Der Greef, J., *Anal. Chem.* **2003**, 75, 4272.

12. Wang, J.; Ibanez A.; Chatrathi, M. P., *J. Am. Chem. Soc.* **2003**, 125, 8444.

13. Wimalasena, R.; Audus , K.L.; Stobaugh, J.F., *Biomed. Chromatogr.* **2003**, 17, 165.

14. Ishii, K., *Chromatography* **2002**, 23, 9.

15. Hirowatari, Y.; Kurosawa, H.; Yoshida, H.; Doumitu, K.-i.; Tada, N., *Anal. Biochem.* **2002**, 308, 336.

16. Cardenosa, R.; Mohamed, R. M.; Aguila, M., *J. Agric. Food Chem.* **2002**, 50, 3390.

17. Aliani, M.; Farmer, L.J., *J. Agric. Food Chem.* **2002**, 50, 2760.

18. Chen, J.G.; Logman, M.; Weber, S.G., *Electroanalysis* **1999,** 11, 331.

19. Chen, J.G.; Woltman, S.J.; Weber, S.G., *J. Chromatogr. A* **1995**, 691, 301.

20. Woltman, S.J.; Chen, J.G.; Weber, S.G.; Tolley, J.O., *J. Pharm. Biomed. Anal.* **1995**, 14, 155.

21. Woltman, S.J.; Even, W.R.; Sahlin, E.; Weber, S.G., *Anal. Chem.* **2000**, 72, 4928.

22. Harmon, B.J.; Gu, X.; Wang, D.I.C., *Anal. Chem.* **1996**, 68, 1465.

23. Tanaka, D.A.P.; Alvarado, M.S.C.; Tanco, M.A.L.; Takahashi, Y.; Chatterjee, A.; Suzuki, H.; Suzuki, T.M., *Anal. Sci.* **2005**, 21, 417.

24. Kitamaki, Y.; Takeuchi, T., *Anal. Sci.* **2004**, 20, 1399.

25. Dikunets, M.A.; Elefterov, A.I.; Shpigun, O.A., *Anal. Lett.* **2004**, 37, 2411.

26. Kitamaki,Y.; Jin, J.Y.; Takeuchi, T., *J. Pharm. Biomed. Anal.* **2003**, 30, 1751.

27. Miura, Y.; Hatakeyama, M.; Hosino, T.; Haddad, P.R., *J. Chromatogr. A* **2002**, 956, 77.

28. Huber, J.F.K.; Jonker, K.M.; Poppe, H., *Anal. Chem.* **1980**, 52, 2.

29. Kucera, P.; Umagat, H., *J. Chromatogr.* **1983**, 255, 563.

30. Nirode, W.F.; Staller, T.D.; Cole, R.O.; Sepaniak, M.J., *Anal. Chem.* **1998**, 70, 182.

31. Cepas, J.; Silva, M.; Perez-Bendito, D.F., *Anal. Chem*. **1995**, 67, 4376.

32. Haginaka , J.F., *Bunseki* **1988**, 131.

33. Selavka, C.M.; Jiao, K.S.; Krull, I.S., *Anal. Chem.* **1987**, 59, 2221.

34. Priebe, S.R.; Howell, J.A., *J. Chromatogr.* **1985**, 324, 53.

35. Vratny, P.; Brinkman, U.A.T.; Frei, R.W., *Anal. Chem.* **1985**, 57, 224.

36. Sahlin, E.; Beisler, A.T.; Woltman, S.J.; Weber, S.G., *Anal. Chem.* **2002**, 74, 4566.

37. Jung, M.C.; Weber, S.G., *Anal. Chem.* **2005**, 77, 974.

38. Kennedy, R.T.; Jorgenson, J.W., *Anal. Chem.* **1989**, 61, 1128.

39. Weber, S.G.; Carr, P.W., *Chemical Analysis*, **1989,** 89, 1.

40. Probstein, R.F., *Physicochemical Hydrodynamics: An Introduction*, John Wiley and Sons, Inc, NY**, 2003**.

41. Knox, J.H.; Gilbert, M.T., *J. Chromatogr.* **1979**, 186, 405.

Chapter 4. Effect of an Open Tube in Series with a Packed Capillary Column on Liquid Chromatographic Performance. The Influence of Particle Diameter, System Pressure, and Temperature.

This work has been published on *J. Chromatogr. A* **2009**, 1216, 1346-1352.

4.1 Introduction

It is well known that postcolumn reactions can improve sensitivity and selectivity in liquid chromatographic analysis[1-3]. Although postcolumn dead volume is not always deleterious to a separation, when the highest efficiency-per-time is needed, postcolumn dead volume may be limiting. Thus, postcolumn reactors come with some disadvantages. The most obvious are the additional hardware and reagents required, and the bandspreading associated with the additional mixing following the separation. The bandspreading issue has been addressed theoretically[4] as well as ex perimentally[5,6]. Optimization of postcolumn conditions for chemiluminescence detection has been achieved[7]. Much of the published work applies to columns with typical dimensions of 4.6 mm ID, 10-20 cm long with 5 μm diameter particles.

In the past several years, HPLC has taken a dramatic step towards fast separations. Both the A term and the C term of the van Deemter equation decrease as d_p decreases. This drives the need for higher pressure capability because the smaller d_p increases back pressure at constant velocity. High pressure pumps permit the application of smaller d_p and higher flow rate at the same time. Numerous particles with sub-2 μm diameter and superior mechanical and chemical stability are present in the market[8]. High temperature HPLC has also attracted interest[8-11]. High temperature decreases the viscosity of the mobile phase and accelerates mass transfer, both of which can lead to faster separations without sacrificing column efficiency[12]. Among the commercially available sub-2 μm packing particles, BEH-C_{18}[13], BEH-Shield RP_{18} [10] and Zorbax Stable Bond particles[14] (Zorbax SB-C_{18}, -C_8, CN, C_3, -Phenyl) have shown excellent thermal stability. Thanks to these emerging materials, high temperature becomes a very promising parameter in HPLC for fast analysis. These advances help to speed up HPLC and shorten

analysis time to minutes or even seconds rendering HPLC a potential method for on-line monitoring and high-throughput analysis.

In a previous paper[15], we studied the influence of the radius of an open tube reactor, which we call a Capillary Taylor Reactor or CTR, on the performance of capillary liquid chromatography where the linear flow rate of the mobile phase is the optimum and the solute k' is 0. The choice of the reactor radius actually depends on several factors such as particle size, maximum available pressure, and column diameter. With a maximum pressure of 4000 psi and for packing particles larger than or equal to 2 μm, the CTR is suitable for columns with radii less than 150 μm ("suitable" is defined as $N_{obs}/N_0 > 90\%$ where N_{obs} is the column efficiency with a CTR while N_0 is that without a CTR). A reactor with a 12.5 μm radius (i.e., commercially available 25 μm ID capillary) works well under such conditions. For 1 μm particles, the requirements are more stringent. However, the assumptions of operating at the optimum velocity and with $k' = 0$ are unrealistic. Therefore, it is necessary to ask: how does a CTR affect the performance of a capillary column in fast separations under realistic conditions?

We will use the Poppe plot, simple but powerful, to analyze our results. It is a log-log plot of the plate time (time equivalent to a theoretical plate, TETP, t/N) vs. the plate number (the number of theoretical plates, N)[16]. Isochrones of constant t are easily drawn on the same plot. Thus, a Poppe plot directly gives not only the number of theoretical plates under certain conditions but also the related analysis time (if k' is known). Short analysis time and a large number of theoretical plates are both desirable but hard to achieve together. With a Poppe plot, it is easy to consider both of them and make a choice depending on what is more important in a specific experiment: the analysis time or the column efficiency.

In this paper, we derived an equation that defines the observed number of theoretical plates (N_{obs}) from a column and CTR with minimal assumptions. We have focused the study on fast separations by investigating three emerging, important parameters in fast HPLC, namely small porous packing particles, high temperature, and high obtainable pressure. By comparing the column efficiency with and without a reactor, we have found that a 5 μm radius reactor is the best for unretained or slightly retained solutes at room temperature. At elevated temperature, the much more practical 12.5 μm radius reactor works. A 12.5 μm radius reactor is actually slightly better than a 5 μm reactor for retained solutes.

4.2 Scheme of the Set Up of a Packed Capillary Column in Series with a CTR

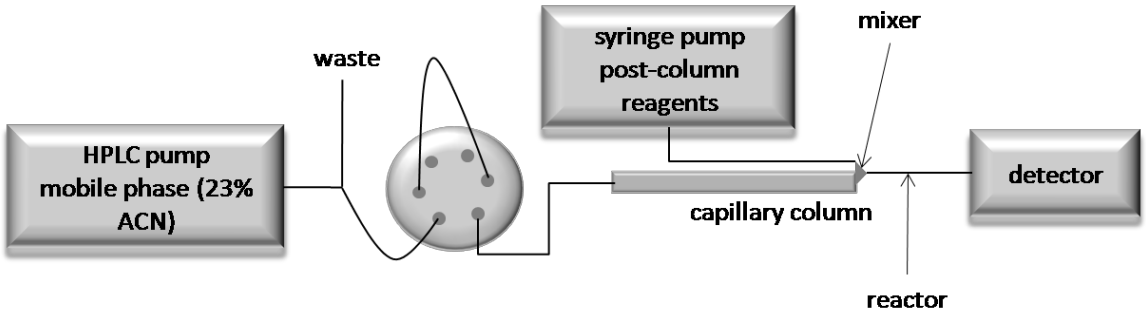

Figure 4.1 Scheme of the set up of a packed capillary column in series with a CTR.

4.3 Theory

A CTR affects column efficiency in two ways: adding band-spreading and requiring pressure. There is no doubt that adding band-spreading damages column efficiency. For a sy stem operating at the maximum attainable pressure, sharing pressure decreases performance for the following reason. A higher pressure drop across the reactor leads to less pressure available for the column which forces a decrease in the linear velocity (longer analysis time) or the length of the column (fewer theoretical plates). The latter problem gets worse for reactors with small radius. Therefore, we derived N_{obs}, the observed number of theoretical plates considering these two effects from a reactor as follows.

4.3.1 The Linear Velocity in the Column in the Presence of a CTR

The total pressure in the system is given by Eq. (1). The first term on the right side of equation is the pressure drop in the column while the second term is the pressure drop across the reactor.

$$P_m = \frac{\phi \eta u_c L_c}{d_p^2} + \frac{8 \eta u_r L_r}{a_r^2} \qquad (1)$$

In Eq. (1), P_m is the maximum pressure provided by the pump; ϕ is the column permeability; η is the viscosity of the mobile phase; a_r is the radius of the capillary used to make the reactor; u_c and u_r are the average linear velocities in the column and the reactor, respectively; L_c and L_r represent the length of the column and the reactor, respectively. The value of ϕ ranges from 500 to 1000 for various columns[17], and we routinely obtain a value of 750 for 2.6 ~ 5 μm particle packed columns with a diameter of 100 μm. Changing ϕ has a negligible effect on the choice of reactor radius as described in a previous paper [15]. u_r can be written as a function of u_c as

$$u_r = \frac{4}{3} u_c b (\frac{a_c}{a_r})^2 \quad (2a)$$

$$b = \varepsilon_e + (1 - \varepsilon_e)\varepsilon_i \quad (2b)$$

When mixing, a post column reagent flow is introduced into the reactor capillary, increasing the flow rate. In our laboratory, the reagent flow rate is set to be 1/4 ~ 1/2 of the column flow rate to obtain the best sensitivity. Here, we chose 1/3. That is the origin of the constant, 4/3, in Eq. (2a). The column radius is a_c ; ε_e is the extraparticle porosity and ε_i is the intraparticle porosity. Both porosities are around 0.4 [18], consequently *b* is 0.64.

The following relationships hold for L_c and L_r

$$L_c = u_c t_0 \quad (3)$$

$$L_r = y u_r a_r^2 / D \quad (4)$$

where t_0 represents the void time of a separation and *y* describes the degree of mixing by diffusion. More complete mixing has a larger *y* value. We chose a value of 2.5 here. This value gives a reactor length that results in a dispersion coefficient defined by the Taylor equation[19]. When the capillary is operating in the Taylor region, the length must be sufficient for an effectively complete reaction if the reaction rate is not the limiting factor[20]. Chemical kinetic factors are not considered here. *D* is the diffusion coefficient of the solute in the mobile phase.

Combining Eqs. (1)-(4), we obtain the expression to define the average linear velocity in column:

$$u_c = \sqrt{\frac{P_m}{\phi \eta t_0 / d_p^2 + \frac{320}{9} \eta b^2 (a_c / a_r)^4 / D}} \quad (5)$$

The viscosity of the mobile phase in units of Pa·s is a function of temperature *T* (in Kelvin) as shown in Eq. (6)[21].

$$\eta(T) = 10^{-5.063+(\frac{602}{T})+0.071x_{acn}+(\frac{62}{T})x_{acn}+0.504x_{acn}^2-(\frac{346}{T})x_{acn}^2} \quad (6)$$

where x_{acn} is the volume percentage of acetonitrile in the mobile phase. We chose 23% in this paper. Another factor dependent on temperature is D, the diffusion coefficient of the solute in the mobile phase,

$$D(T) = D_0(T_0)\frac{\eta_0(T_0)T}{\eta(T)T_0} \quad (7)$$

which is derived from the Walden product, $D\eta/T = \text{constant}$. In this paper, we chose D_0 to be 7.0×10^{-10} m^2/s at 293 K to represent a low molecular weight solute.

With moderate manipulation, an expression for u_c is obtained as a function of P_m, d_p, a_r, a_c, t_0 and T as shown in Eq. (8).

$$u_c(P_m, d_p, a_r, a_c, t_0, T) = \sqrt{\frac{P_m}{\phi\eta(T)t_0/d_p^2 + \frac{320}{9}\eta(T)b^2(a_c/a_r)^4/D(T)}} \quad (8)$$

4.3.2 Column Efficiency with a CTR

We used the van Deemter equation to define H_c, the height equivalent to a theoretical plate, for the case in which the 'C term' is dominated by intraparticulate mass transfer.

$$H_c(P_m, d_p, a_r, a_c, t_0, T, k'') = \frac{2D(T)}{u_e} + \lambda d_p + \frac{d_p^2}{gD(T)}u_e\frac{k''}{(1+k'')^2} \quad (9)$$

where λ and g are numerical, geometry-dependent constants. Typically λ is 2 and g is 30[18] for spherical particles. u_e is the extraparticle linear velocity and k'' is the zone capacity factor. k'' relates to k', the retention factor, by $k'' = k_0 + (1+k_0)k'$, where k_0 is equal to $(1-\varepsilon_e)\varepsilon_i/\varepsilon_e$, and

has a constant value of 0.6 if the porosities are set to 0.4. The extraparticle velocity u_e is defined as $(1+k_0)u_c$.

H_c can be calculated provided that u_c is known from Eq. (8). The variance from a column in the units of time squared then can be determined by Eq. (10).

$$\sigma_{c,t}^2(P_m, d_p, a_r, a_c, t_0, T, k'') = \frac{H_c L_c}{u_e^2}(1+k'')^2 = \frac{H_c t_0}{(1+k_0)^2 u_c}(1+k'')^2 \tag{10}$$

Eq. (11) is H_r, the height equivalent to a theoretical plate in a reactor[1].

$$H_r(a_r, T) = u_r a_r^2 / 24D(T) \tag{11}$$

The variance in time units for a reactor is given by (using Eqs. (4) and (11))

$$\sigma_{r,t}^2(a_r, T) = \frac{H_r L_r}{u_r^2} = \frac{u_r a_r^2}{24D(T)} \frac{2.5 u_r a_r^2}{D(T)} \frac{1}{u_r^2} = \frac{2.5 a_r^4}{24D(T)^2} \tag{12}$$

Therefore, the observed number of plates, N_{obs}, including both effects of the reactor, is expressed as

$$N_{obs}(P_m, d_p, a_r, a_c, t_0, T, k'') = \frac{(t_e(1+k'')+t_r)^2}{\sigma_{c,t}^2 + \sigma_{r,t}^2} = \frac{(t_0(1+k'')/(1+k_0)+t_r(a_r, T))^2}{\sigma_{c,t}^2 + \sigma_{r,t}^2} \tag{13}$$

where t_e is the dead time for a species that remains in the flowing mobile phase and t_r is the time to pass through the CTR: $t_r(a_r, T) = L_r / u_r = y\frac{a_r^2}{D(T)}$.

For the sake of clarity, an example is given here to illustrate the calculation. With a d_p of 1.7 μm, an a_r of 12.5 μm, an a_c of 50 μm, a t_0 of 5 s, a T of 293 K and a P_m of 4000 psi, we calculated the average linear velocity to be 4.5×10^{-3} m/s based on Eq. (8). We then obtained the

values of H_c, $\sigma_{c,t}^2$ and $\sigma_{r,t}^2$ for an unretained component (k''= 0.6) according to Eqs. (9), (10) and (12) as 3.8 $\times 10^{-6}$ m, 4.3×10^{-3} s^2 and 5.6×10^{-3} s^2, respectively. Finally, we calculated N_{obs} and t/N_{obs} based on Eq. (13). They are 3155 and 1.8 $\times 10^{-3}$ s. For a set of t_0 values, we obtain a set of N_{obs} and t/N_{obs} values which results in one Poppe plot.

4.3.3 Column Efficiency Without a CTR

To display the effect of the reactor, we also calculate the number of theoretical plates under the same conditions but without the reactor (N_0) as shown below. The derivation procedure is similar to the one with the reactor but it ignores the reactor part.

$$u_0(P_m, d_p, t_{0,} T) = \sqrt{\frac{P_m d_p^2}{\phi\eta(T) t_0}} \tag{14}$$

$$L_0(P_m, d_p, t_0, T) = u_0 t_0 \tag{15}$$

$$H_0(P_m, d_p, t_0, T, k^{"}) = \frac{2D(T)}{u_{e0}} + \lambda d_p + \frac{u_{e0} d_p^2}{gD(T)} \frac{k^{"}}{(1+k^{"})^2} \tag{16}$$

$$\begin{aligned} N_0(P_m, d_p, t_0, T, k") &= L_0 / H_0 \\ &= u_0 t_0 / H_0 \end{aligned} \tag{17}$$

where u_{e0} is defined as $(1+k_0)u_0$.

4.4 Assumptions and Approximations

As in any approach to a quantitative analysis of a complex system, approximations and assumptions have been made. There are four choices we have made that require at least a brief

discussion; namely, the reagent flow rate, the choice of what expression to use for plate height, whether Taylor dispersion is a good description of what occurs in the reactor, and what diffusion coefficient to use.

First, let us consider the reagent flow rate. There is not a correct choice here, but it is certainly true that using a minimal flow rate is best to avoid dilution. Consequently, we have chosen the flow rate of the reagent to be 1/3 of that of the column. This happens to match the current practice in our laboratory. Next, let us consider which bandspreading equation to use. Here we made two choices. First, we chose the van Deemter equation. Furthermore, we chose to take only a single C-term representing intraparticle diffusion. Both of these choices can be criticized from the perspective that they may not be accurate for a particular set of circumstances. In our view, there are several reasons to support these choices. For one thing, the choice is convenient. To the degree that one would like to manipulate algebraic expressions for understanding, it becomes easier with the algebraically simple van Deemter equation, as it has no fractional powers of velocity. Also, we have a previous related publication using the same van Deemter equation. Continuing to use the van Deemter equation makes the comparison of this work and the published work more convenient. Finally, and most importantly, the choice does not matter much. For the most part, in this work we will compare performance of a column with a reactor to a column without a reactor. Further, we mostly focus on changes induced by altering temperature and pressure, and those effects as a function of reactor capillary radius, and over 2-3 orders of magnitude of time (t_0). For this broad perspective, the differences among the approaches to describe H disappear. Last, we must consider issues surrounding the use of Taylor dispersion to describe bandspreading in the tubular post-column reactor. When experimental conditions are in the Taylor dispersion region, a uniform mixing zone without a radial

concentration gradient will be formed. Therefore, in the Taylor region, the reagent stream and the analyte stream will be thoroughly mixed. We have assumed a rapid reaction, rapid enough that reaction occurs faster than mixing. Under this assumption, the reactor's efficacy is related to the system being adequately described by Taylor dispersion. There are two criteria for being in the Taylor region: $Pe = ua/D > 70$, which guarantees the axial molecular diffusion is negligible compared to the total dispersion effect (that is, the system is not in the Taylor-Aris region), and $Pe < 0.4\ L/a$ to make sure that the reactor tube is long enough for the diffusion to relax the radial concentration gradient[19]. In our calculations, the reactor length is chosen to satisfy the criterion that *Pe* equals $0.4\ L/a$ (Eq. 4 above). Under all the conditions that we will explore below, *Pe* is larger than 70, so the reaction capillary is theoretically in the Taylor region. We have already demonstrated that the reactors obey Taylor dispersion theory[1], and the bandbroadening contribution from the mixing portion of the reactor (*i.e.*, the point of mixing of the streams, changes in tubing diameter etc.) is actually immeasurable. Thus, the reactor behaves like a Taylor reactor theoretically and experimentally. There is one final caveat and discussion that is related to the diffusion coefficient. The caveat is that the calculations below assume a fairly small molecule. The results may be different if the solute is a 100 kDa protein, for example. The discussion is related to the fact that there are actually two important diffusing species, the solute that elutes from the column and its reaction product (creating a detectable species). We have assumed that the diffusion coefficients of the solute and the detected species are the same. For example, we use Cu(II) as a reagent for peptides[22]. The small change in molecular weight will not alter the diffusion coefficient considerably. Finally, we have assumed that the diffusion coefficient does not change when the chromatographic eluent and the reagent stream combine.

This may or may not be significant, depending on the actual conditions. In this paper, we have not incorporated this effect because there is little to be gained from the added complexity.

4.5 Result and Discussion

4.5.1 The Effect of a 25 μm CTR on the Performance of HPLC

Before turning to Poppe plots, it is informative to understand the magnitude of the problem. Figure 4.2 shows the effect of a reactor with a radius of 25 μm (which is easily fabricated in the laboratory) on the column efficiency. N_{obs}, defined by Eq. (13), is the number of theoretical plates with the reactor's effects taken into account while N_0, defined by Eq. (17), is the number of theoretical plates generated by the same column but without a reactor. When N_{obs}/N_0 is greater than or equal to 90%, we consider the effect of the reactor to be acceptable throughout this paper. As shown in Figure 4.2, N_{obs}/N_0 is at best 73% for columns packed with particles of diameters ranging from 1 μm to 5 μm for a separation with a t_0 of 50 s. It becomes even smaller as analysis speed is increased. Column efficiency is reduced to less than 14% at a t_0 of 5 s which is not tolerable. Thus, it is necessary to optimize the conditions to minimize the effect from a CTR especially when speed is required.

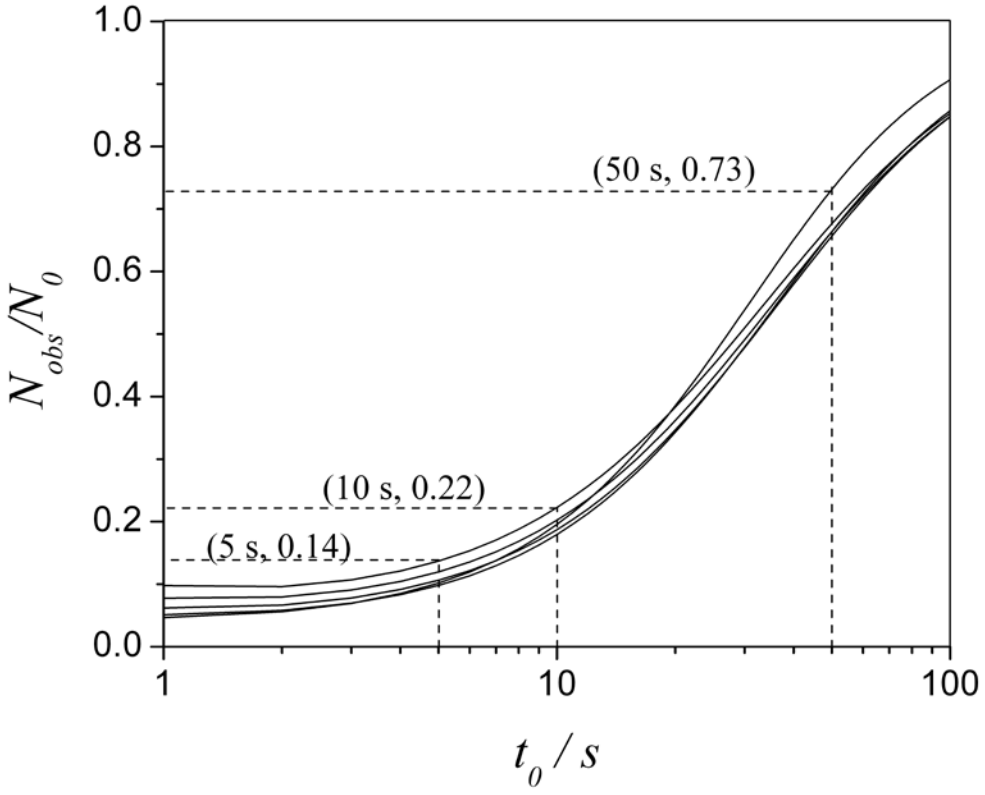

Figure 4.2 The effect of a 25 μm CTR on column efficiency (N_{obs}/N_0 vs t_0) when the packing particle diameter ranges from 5 μm to 1 μm (up to bottom from the left). Conditions are as follows: P_m = 4000 psi; b = 0.64; φ = 750; g = 30; λ= 2; a_c = 50 μm; a_r = 25 μm; T = 293 K; k'' = 0.6 (k'= 0).

4.5.2 Optimization of CTR Radius

The effect of reactor radius on efficiency is shown in Figure 4.3. The curves representing the four reactors are all more or less far away from the dashed line (no reactor) with a short analysis time while becoming closer to the dashed line when the analysis is slower. Some of them even overlap the dashed line when the analysis time is long enough which means that the effect from a

CTR can disappear when the separation is slow enough. Among them, the 5 μm curve is on average closest to the dashed line, especially at small t_0. Therefore, a reactor with a radius of about 5 μm has the least effect on the column efficiency. The 1 μm reactor line is exceptional. It is always far away from the dashed line with a t_0 ranging from 1 to 200 s.

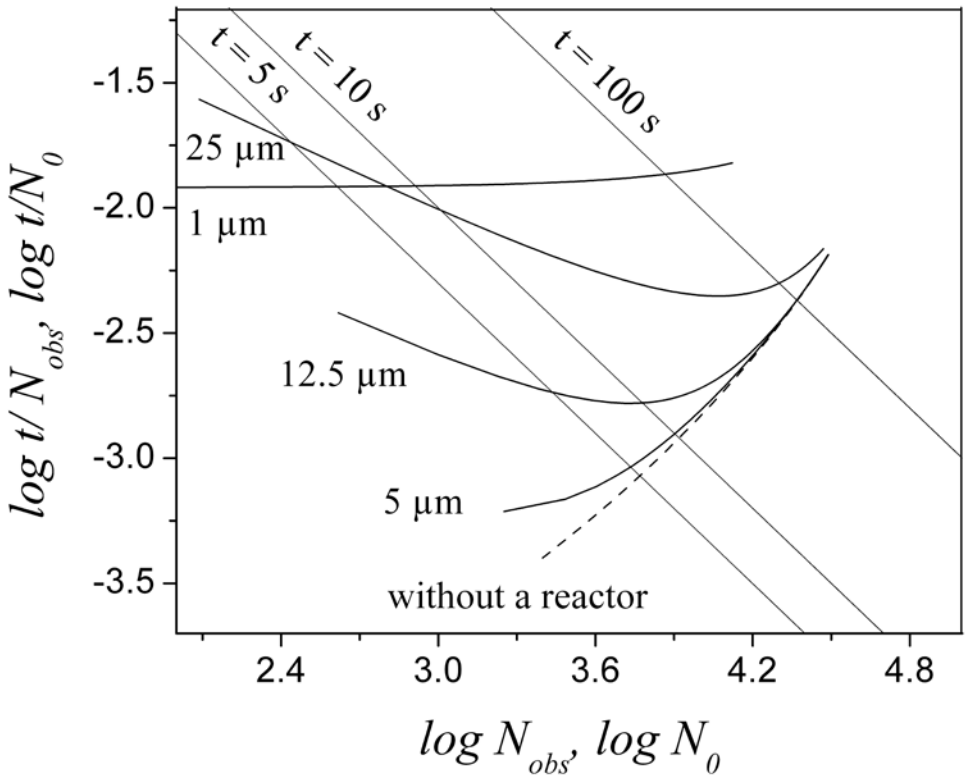

Figure 4.3 Poppe plots for reactors with various radii. d_p= 1.7 μm and other conditions are the same as in Figure 4.2.

Figure 4.4 and Figure 4.5 demonstrate how the reactor affects the column efficiency and how these effects are related to the reactor radius and the analysis time of a separation. P_r is the pressure drop across a reactor (the second term of Eq. (1)). $\sigma^2_{r,t}$ is the variance in the reactor calculated from Eq. (12) and $\sigma^2_{c,t}$ is the variance in the column calculated from Eq. (10).

Obviously, large diameter reactors require less pressure and leave more pressure to the column which in turn gives a better separation (Figure 4.4). On the other hand, large reactors contribute more to bandspreading which hurts the column efficiency (Figure 4.5). However, both effects have one thing in common: they get smaller at longer analysis time. That is, the reactor's effect on the column efficiency is more critical in fast separations.

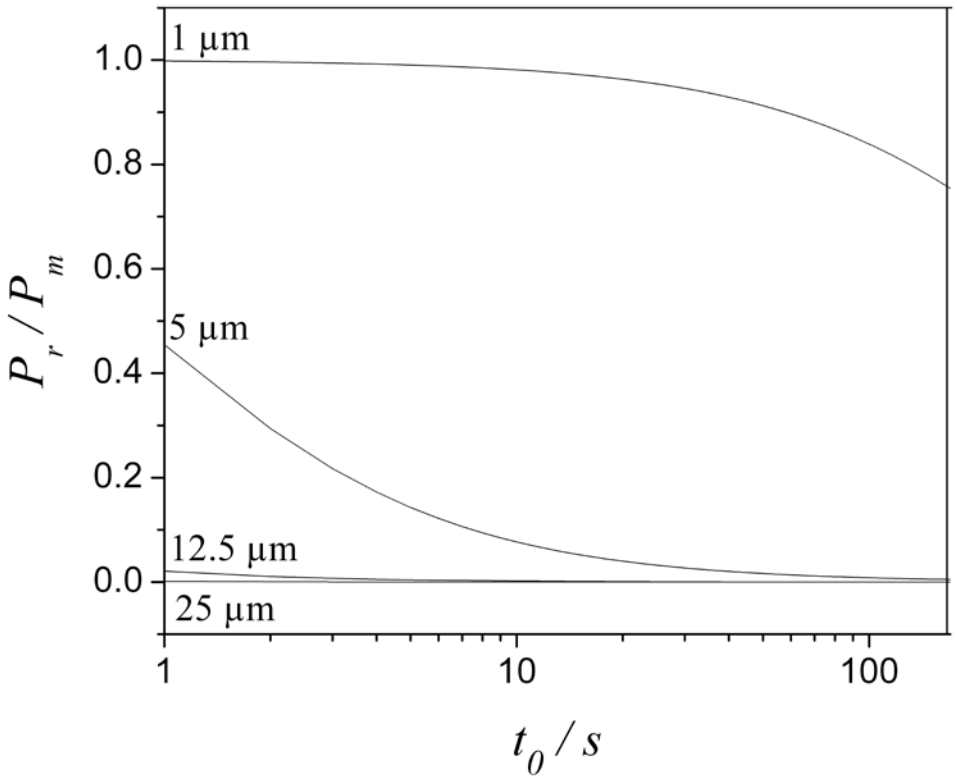

Figure 4.4 Pressure drop across the reactor as a fraction of the attainable pressure as a function of t_0. Curves for various reactor radii are labeled. Other conditions are as the same as in Figure 4.3.

The bandspreading caused by a 1 μm reactor is negligible. The effect of a 1 μm reactor on the column efficiency then mainly comes from the pressure it requires. As shown in Figure 4.4, the pressure drop across a 1 μm reactor is more than 84% of the maximum pump pressure in a t_0 range of 1 s to 100 s. The column efficiency in this case is comparable to that generated on the same column operated at less than 16% of the total pressure in the absence of a reactor. That explains why the 1 μm line (Figure 4.3) is always far from the dashed line (no reactor). On the other hand, the pressure drop across a 25 μm reactor is negligible according to Figure 4.4, so that the effect of a 25 μm reactor on the column efficiency is mostly caused by bandspreading. As shown in Figure 4.5, the band spreading occurring in a 25 μm reactor is almost equal to the total bandbroadening at a t_0 shorter than 10 s and it gradually decreases with an increase of the analysis time. This explains why in Figure 4.3 the 25 μm curve becomes closer to the 'no reactor' curve as the analysis time gets longer. Figure 4.3, 4.4 and 4.5 show that, for large enough t_0, the effects of 5 and 12.5 μm reactors on both pressure and bandspreading are small. For 5 μm reactors, N_{obs}/N_o is greater than 0.93 for a t_0 greater than 5 s. The same is true for 12.5 μm reactors when t_0 is longer than 25 s. Unfortunately, a 5 μm radius reactor would be very difficult to manufacture.

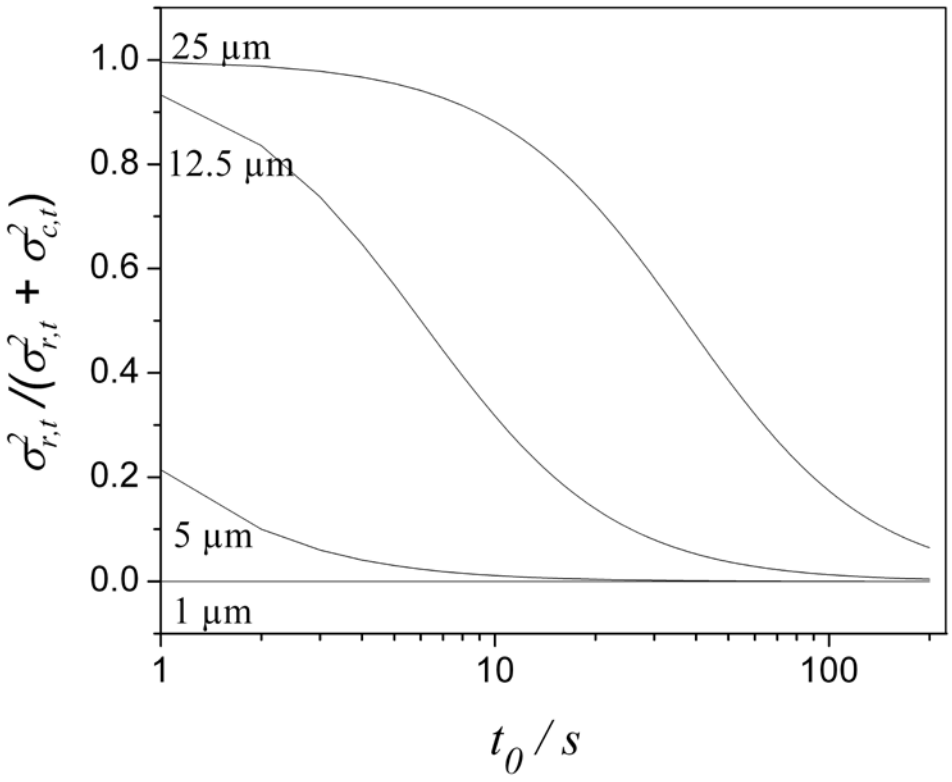

Figure 4.5 Variance in a postcolumn reactor as a fraction of the total variance vs. t_0 for unretained solutes. Curves corresponding to various reactor radii are labeled. The conditions are the same as in Figure 4.3.

4.5.3 Minimize Reactor Effect by Increasing Temperature

Temperature is a very powerful parameter in fast HPLC[12]. The viscosity of the mobile phase decreases at elevated temperature, so does the pressure drop across the reactor. The diffusion coefficient of a solute in the mobile phase increases so that the bandspreading in the reactor decreases for velocities greater than the optimum velocity. Temperature should have an influence on the effect of the reactor on efficiency.

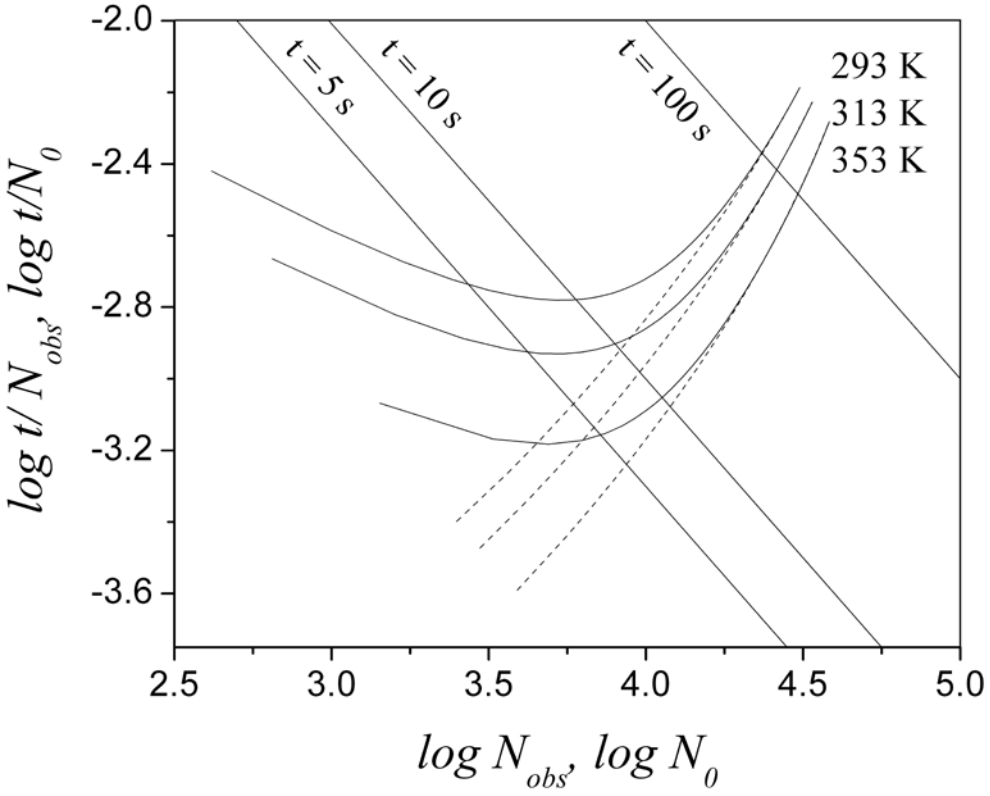

Figure 4.6 Poppe plots at different temperatures. Solid curves represent the results with a 12.5 μm reactor while dashed curves represent those without a reactor. Other conditions are the same as in Figure 4.3.

Figure 4.6 shows Poppe plots at three different temperatures with or without a 12.5 μm reactor. Obviously, increasing the temperature helps to minimize the effect from the reactor because the solid curves are closer to the related dashed line at high temperature at a given analysis time, e.g. t = 10 s. The valule of N_{obs}/N_o increases to 93% at 353 K and a t_0 of 10 s from 73% at 293 K.

Table 4.1 shows the percentage of the total variance that comes from the reactor at four temperatures and three values of t_0. The higher the temperature or the larger t_0 is, the smaller the

effect from the reactor on the bandbroadening. The change in the reactor effect caused by increasing temperature is dramatic. With a t_0 of 5 s, the added bandbroading from a 12.5 µm reactor decreases from 57% to 15% when the temperature is increased from 293 K to 373 K. With a t_0 of 10 s, this number decreases from 32% to 6%. Therefore, high temperature significantly minimizes the effect of a 12.5 µm reactor on bandbroadening which in turn is of benefit to column efficiency.

Table 4.1 Temperature minimizes the effect of a 12.5 µm reactor on bandbroadening. P_m= 4000 psi; b= 0.64; φ= 750; g= 30; λ= 2; a_c= 50 µm; a_r= 12.5 µm; k''=0.6 (k'=0)

	$\sigma_r^2/(\sigma_r^2+\sigma_c^2)$ (%)			
	T = 293 K	T = 313 K	T = 353 K	T = 373 K
t_0 = 5 s	57	42	21	15
t_0 = 10 s	32	21	9	6
t_0 = 30 s	8	5	2	1

4.5.4 Reactor Effect at Different Maximum Pressures

According to the van Deemter equation, the A and C terms decrease as particle size (d_p) decreases. The right side of the van Deemter curve where the C-term dominates becomes flatter indicating that for small d_p, column efficiency is not compromised too much at high velocities. However, small particles and high velocities lead to high pressure drop across the columns suggesting that high pressure is advantageous for fast separations.

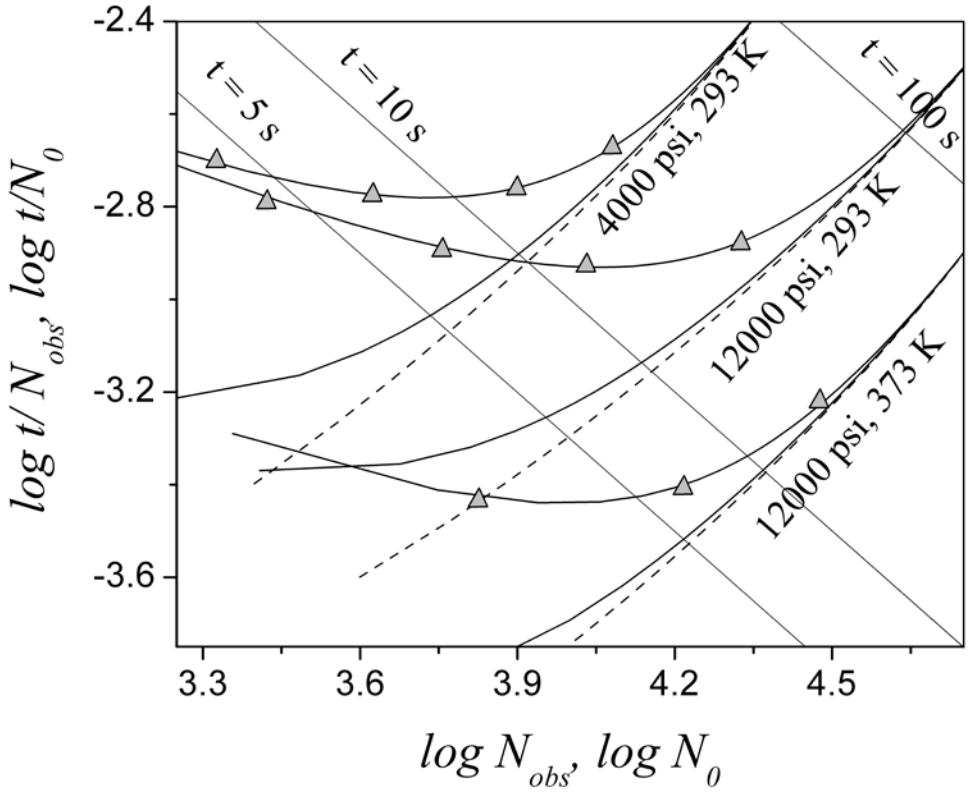

Figure 4.7 Poppe plots at different pressures. Solid line represents the results with reactors (solid line with triangles is with a 12.5 μm reactor; solid line without symbols is with a 5 μm reactor) while dashed line represents those without a reactor. Temperature and pressure are indicated. Other conditions are the same as in Figure 4.3.

Figure 4.7 shows how a CTR impacts column efficiency at various available pressures. Reactors affect the column efficiency in a similar way at all pressures: the effect of a reactor is larger at shorter analysis time. Operating at higher attainable pressure obviously gives better separation without a reactor as the dashed plots show. With a dead time of 5 s and at room temperature, the column efficiency at 12000 psi is almost twice that at 4000 psi. The advantage brought by the high pressure almost disappears with a 12.5 μm reactor at a t_0 of 10 s. The column

efficiency is only 39% of N_0 at 12000 psi with a 12.5 μm reactor with a t_0 of 5 s and it is even worse than that at 4000 psi without a reactor. With a 5 μm reactor, it gets better. The column efficiency only decreases a small amount, from 93 % to 92% of N_0 when pressure increases from 4000 psi to 12000 psi. Increasing the temperature greatly improves the column performance with a CTR, as shown in the bottom set of curves. The effect from a 5 μm reactor almost disappears at 373 K. The column efficiency with a 12.5 μm reactor also exceeds 90% at a t_0 of 10 s at this temperature. Therefore, to maximize the benefit of ultra high pressure, elevated temperature combined with a small radius reactor is certainly preferred.

4.5.5 Reactor Effect is Minimized for Retained Solutes.

Band spreading occurs in the reactor, but it is not significant if the bandspreading on the column is significant. The peak for a retained solute is obviously more broadened than that for an unretained solute. Thus, we have studied the reactor effect when solutes are retained. The results are shown in Figure 4.8 where solid lines represent the contribution of the reactor with various radii to the bandbroadening and dashed lines show the corresponding ratio of column efficiency. The effect of a reactor with smaller radius (1 μm or 5 μm) on bandbroadening is negligible . The bandbroadening effect of a reactor with a manageable radius (12.5 μm or 25 μm) greatly decreases and starts to disappear when retention gets larger. The variance of a 12.5 μm reactor decreases from 32% (k" = 0.6, shown in Figure 4.5) of the total variance to only 5% (k" = 3.8) with a t_0 of 10 s. The situation is almost the same for a 5 μm reactor. Furthermore, a 12.5 μm reactor requires much less pressure than a 5 μm reactor does (shown in Figure 4.4). This implies that a 12.5 μm reactor could be better than a 5 μm reactor for retained solutes in fast separations. This notion is verified by the dashed lines. A 12.5 μm reactor starts to supersede a 5 μm reactor

with a t_0 longer than 5 s when k" equals 3.8 (or k' equals 2). Even a 25 μm reactor is suitable with a t_0 longer than 27 s as indicated by the shaded portion of Figure 4.8.

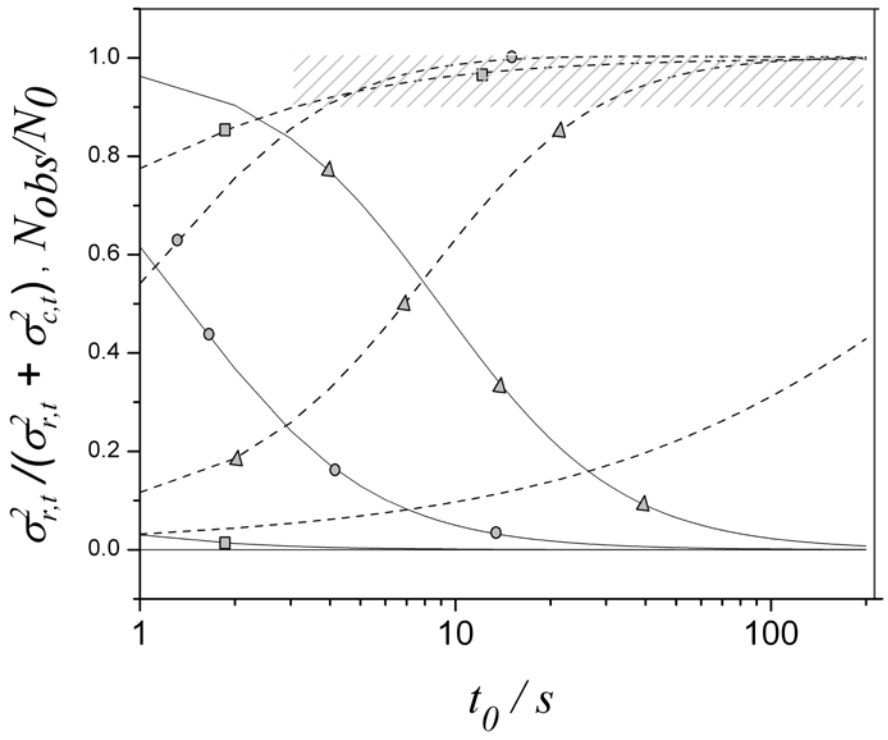

Figure 4.8 Contribution of a reactor with various radii to the band spreading (expressed as $\sigma_{r,t}^2/\left(\sigma_{r,t}^2+\sigma_{c,t}^2\right)$) of moderately retained solutes (k'' = 3.8) (solid line) and corresponding N_{obs}/N_0 (dashed line) with a t_0 ranging from 1 s to 150 s (triangle denotes the 25 μm radius reactor; circle is 12.5 μm; rectangular is 5 μm; no symbol is 1 μm). Shadow indicates where the reactor has negligible effect on column performance. Other conditions are the same as in Figure 4.3.

4.5.6 Practical Limitations

Theoretical calculations demonstrate that high pressure and elevated temperature greatly increases the column efficiency in fast separations not only by allowing the use of small packing

particles and high velocity of the mobile phase at the same time but also by diminishing the reactor effect. High pressure pumps are now commercially available. Particles with superior mechanical,chemical, and thermal stability are present in the market[8, 14]. The fabrication of a CTR is now the only practical limitation. The construction of a CTR was described elsewhere[1]. Briefly, two tungsten wires are each threaded into two capillaries and then both into another capillary. The junction between the three capillaries is then placed into a piece of PTFE/FEP dual shrink/melt tube. When heating, the outer PTFE layer starts shrinking and the inner FEP layer starts melting. After cooling down, the tungsten wires are removed and a CTR is formed. Small tungsten wires curl up leading to the difficulty in preparation of a CTR with small radius. This again explains why we pursue suitable conditions so that a 12.5 μm radius reactor can be used. The other limitation of CTR fabrication is the length. According to our experience, the length of a CTR cannot be shorter than about 1 cm because of the presence of the dual shrink/melt tube.

In this paper, we used Taylor dispersion theory to define the length of the reactor. It is interesting to consider the length of the reactor and the column that arises in a 'high performance' scenario. Figure 4.9 displays the length of a 100 μm (ID) column packed with 1.7 μm particles and a 12.5 μm (radius) reactor at 12000 psi and 373 K and the corresponding number of theoretical plates. It is noteworthy that these conditions lead to about 20,000 theoretical plates at a t_0 of 10 s. Furthermore, both lengths are greater than 2 cm with a dead time shorter than 10 s so that we can directly apply the optimal calculated parameters for such separations. However, for separations with longer t_0 (>10 s), the reactor length needed for complete mixing is actually less than 2 cm in theory. Experimentally, a longer reactor may be preferred for practical reasons which may increase bandbroadening in the reactor. The column efficiency may then be worse than expected from theory.

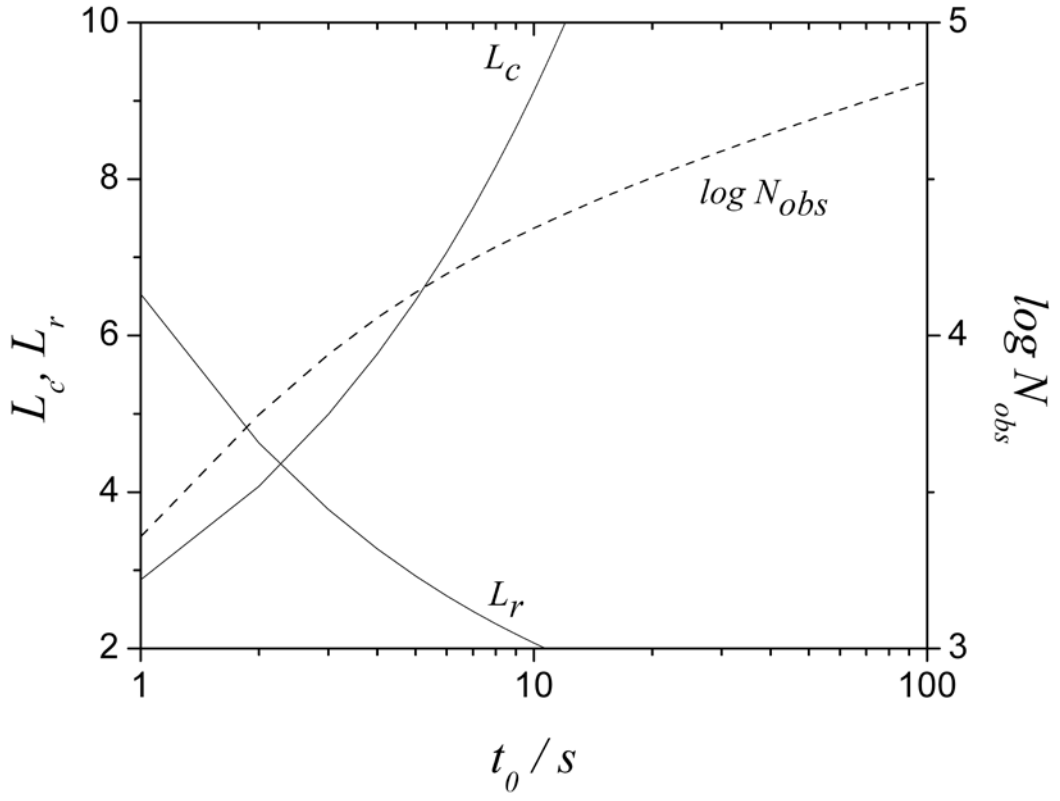

Figure 4.9 Lengths of a reactor with a radius of 12.5 μ m (dashed line) and a 100 μm (ID) column packed with 1.7 μm particles (solid line) and corresponding N_{obs} vs. t_0 at a temperature of 373 K and a pressure of 12000 psi. Other conditions are the same as in Figure4.3.

4.6 Conclusion

A postcolumn open capillary, including a postcolumn reactor, steals pressure from the column which in turn decreases the number of theoretical plates when a small radius capillary is used. At the same time, it adds band broadening especially when a large radius capillary is used. Such

effects become more intolerable as the separation goes faster. For a 1.7 μm d_p column (100 μm ID) with a pressure of 4000 psi and at room temperature, a 5 μm radius reactor is the best for unretained species, but such a small radius reactor is hard to fabricate and maintain. Fortunately, higher temperature helps to minimize the reactor's effect so that an easily fabricated 12.5 μm radius reactor is suitable in fast separations. The reactor's effect is relatively smaller for retained species due to their larger on-column band broadening compared to unretained species. For a moderately retained species, a 12.5 μm reactor becomes even better than a 5 μm reactor at a t_0 longer than 5 s when other conditions are the same. Ultra-high pressure greatly increases the column efficiency but this benefit is lost especially for unretained or slightly retained species when a 12.5 μm reactor is used. To take full advantage of high pressure with a 12.5 μm reactor, higher temperature is a must. At a t_0 of 5 s, a pressure of 12000 psi, room temperature and with a 12.5 μm reactor, N_{obs}/N_0 is only 39% for an unretained solute. Under the same conditions but at a temperature of 373 K, N_{obs}/N_0 increases to 81% and 99% for unretained and moderately retained solutes (k" = 3.8, k' = 2), respectively. Therefore, a capillary HPLC column followed by a CTR with manageable radius (larger than 12.5 μm) gives best column efficiency for moderately or strongly retained solutes at high pressure coupled with high temperature.

Reference

1. Beisler, A.T.; Sahlin, E.; Schaefer, K.E.; Weber, S.G., *Anal. Chem.* **2004**, 76, 639.
2. Brinkman, U.A.T., *Chromatographia* **1987,** 24, 190.
3. M.K. Freeman, Daunert, S. Bachas, L.G., *LC-GC* **1992**, 10, 112.

4. Huber, J.F.K.; Jonker, K.M.; Poppe, H., *Anal. Chem.* **1980**, 52, 2.

5. Kucera, P.; Umagat, H., *J. Chromatogr. A* **1983**, 255, 563.

6. Nirode, W.F.; Staller, T.D.; Cole, R.O.; Sepaniak, M.J., *Anal. Chem.* **1998**, 70, 182.

7. Cepas, J., Silva, M.; Perez-Bendito, D., *Anal. Chem.* **1995**, 67, 4376.

8. Majors, R.E., LC-GC **2008**, 26, 16.

9. Heinisch, S.; Desmet, G.; Clicq, D.; Rocca, J.-L., *J. Chromatogr. A* **2008**, 1203, 124.

10. Nguyen, D.T.-T.; Guillarme, D.; Heinisch, S.; Barrioulet, M.-P.; Rocca, J.-L.; Rudaz, S.; Veuthey, J.-L., *J. Chromatogr. A* **2007**, 1167, 76.

11. Xiang, Y . Liu, Y.; Lee, M.L., *J. Chromatogr. A* **2006**, 1104, 198.

12. Yang, X.; Ma, L.; Carr, P.W., *J. Chromatogr. A* **2005**, 1079, 213.

13. F. Gritti, G. Guiochon, *J. Chromatogr. A* **2008**, 1187, 165.

14. D. Guillarme, R. Russo, S. Rudaz, C. Bicchi, J.-L. Veuthey, Curr. Pharmaceut. Analysis **2007**, 3, 221.

15. H. Xu, S.G. Weber, *J. Chromatogr. A* **2006**, 1113, 116.

16. Poppe, H., *J. Chromatogr. A* **1997**, 778, 3.

17. Knox, J.H.; Gilbert, M.T., *J. Chromatogr.* **1979**, 186, 405.

18. Weber, S.G.; Carr, P.W., *Chemical Analysis* (New York, NY, United States) 1989, 98, 1.

19. Probstein, R.F., *Physicochemical Hydrodynamics: An Introduction*, 2nd Edition, **2003**.

20. Jung, M.C.; Weber, S.G., *Anal. Chem.* **2005**, 77, 974.

21. Cabooter, D.; Heinisch, S.; Rocca, J.L.; Clicq, D.; Desmet, G., *J. Chromatogr. A* **2007**, 1143, 121.

22. Chen, J.G.; Logman, M.; Weber, S., *Electroanalysis* **1999**, 11, 331.

Conclusion

We have developed a novel sampling method based on electroosmosis and applied it to draw physiological fluid through the extracellular space of an OHSC. We have characterized this new sampling method by measuring the flow rate, examining the use of internal standards, and examining cell death caused by sampling. The sampling flow rate ranges from 60 to 150 nL/min with a 150 μm (ID) sampling capillary and an electric field (at the tip of the capillary) from 30 to 60 V/cm. Cell death can be negligible for a sampling time of 5 min at a moderate electric field with the sampling capillary tip 50 μm away from the slice culture surface. Using this sampling approach, we have electroosmotically pulled Leu-enkephalin through OHSCs to identify ectopeptidase activity in the CA3 region. These studies show that a bestatin-sensitive aminopeptidase may be critical for the hydrolysis of exogenous Leu-enkephalin, a neuropeptide present in the CA3 region of OHSCs.

We have not determined the spatial resolution here quantitatively. We estimate, based on the images of tissue damage (when it occurs) that the spatial resolution is on the order of several hundred micrometers. This will need to be studied more rigorously in the future.

Electroosmotic sampling appears to be effective. The approach is simple and ideal for sampling through slices with a thickness of only 150 μm and from the surface of an organ as well. *In vivo* application can be envisioned with narrower or pulled capillaries. Electroosmotic

sampling could be employed to study ectopeptidase activity in intact tissue with high spatial resolution. Electoosmotic sampling also could find its application in extracellular endogenous peptide extraction and determination when combined with appropriate quantitative analytical approaches.

We have investigated the effect of a postcolumn open capillary, including a postcolumn reactor, on the performance of a capillary column. A capillary Taylor reactor (CTR) steals pressure from the column which in turn decreases the number of theoretical plates when a small radius capillary is used. At the same time, CTR adds band broadening especially when a large radius capillary is used. Such effects become more intolerable as the separation goes faster. For a 1.7 μm d_p column (100 μm ID) with a pressure of 4000 psi and at room temperature, a 5 μm radius reactor is the best for unretained species, but a reactor with such a small radius is hard to fabricate and maintain. Fortunately, higher temperature helps to minimize the reactor's effect so that an easily fabricated 12.5 μm radius reactor is suitable in fast separations. The reactor's effect is relatively smaller for retained species due to their larger on-column band broadening compared to unretained species. For a moderately retained species, a 12.5 μm reactor becomes even better than a 5 μm reactor at a t_0 longer than 5 s when other conditions are the same. Ultra-high pressure greatly increases the column efficiency but this benefit is lost especially for unretained or slightly retained species when a 12.5 μm reactor is used. To take full advantage of high pressure with a 12.5 μm reactor, higher temperature is a must. At a t_0 of 5 s, a pressure of 12000 psi, room temperature and with a 12.5 μm reactor, N_{obs}/N_0 is only 39% for an unretained solute. Under the same conditions but at a temperature of 373 K, N_{obs}/N_0 increases to 81% and 99% for unretained and moderately retained solutes (k" = 3.8, k' = 2), respectively. Therefore, a capillary HPLC column followed by a CTR with a manageable radius (larger than 12.5 μm)

gives the best column efficiency for moderately or strongly retained solutes at high pressure coupled with high temperature.

Supplemental Information

Derivation of reaction rate (*k*)

1. The moles of internal standard (IS) collected

   $mol_{IS} = U \times t_s \times [IS]$ (1)

   Where *U* is the sampling flow rate, t_s is sampling time and *[IS]* is the initial concentration of IS in bath.

   $mol_{IS} = A_{IS}/f_{IS}$ (2)

   A_{IS} is the peak area of IS and f_{IS} is a calibration factor. Thus, *U* can be expressed as follows,

   $U = A_{IS}/([IS] \times t_s \times f_{IS})$ (3)

2. Exposure time of peptide to tissue, t_e

   $t_e = V_t/U$ (4)

   V_t is the volume of tissue sampled. By substituting Eq. (3) and Eq. (2) into Eq. (4), we obtained

   $t_e = V_t \times f_{IS} \times t_s \times [IS]/A_{IS}$ (5)

   and

   $t_e = V_t \times t_s \times [IS]/mol_{IS}$ (5a)

3. The moles of substrate/product consumed/produced per unit time with initial rate assumption

$$k = v_{max}/(K_m + [s]) \quad (6)$$

$$\frac{\Delta[s]}{\Delta t} = -k[s] = ([s] \times v_{max})/(K_m + [s]) \quad (7)$$

Thus, the concentration of substrate leaving the tissue $[s]_o$ can be expressed as follows,

$$[s]_o = [s]_i - k \times [s]_i \times t_e \quad (8)$$

or

$$[s]_o = [s]_i(1 - kt_e) \quad (9)$$

$[s]_i$ is the concentration of substrate entering into the tissue.

From Eq. (8) or Eq. (9), we obtained

$$k = (1 - \frac{[s]_o}{[s]_i})/t_e \quad (10)$$

$$[s]_o = \frac{mol_{s,o}}{mol_{IS}/[IS]} \quad (11)$$

Here $mol_{s,o}$ is the moles of substrate leaving out of the tissue. When substituting Eq. (5a) and (11) into Eq. (10),

$$k = \frac{mol_{IS}}{[IS]\times V_t \times t_s} - \frac{mol_{s,0}}{[s]_i \times V_t \times t_s} \quad (12)$$

Therefore, from the decreasing of YGGFL (the substrate) we have

$$k = \frac{A_{IS}}{f_{IS}\times[IS]\times V_t \times t_s} - \frac{A_{s,o}}{f_s \times [s]_i \times V_t \times t_s} \quad (13)$$

In Eq. (13), $[IS]$, $[s]_i$, V_t and t_s are given experimental conditions. Here we assume the sampling volume in the tissue is a cylinder. A_{IS}, $A_{s,o}$, f_{IS} and f_s can be obtained from the analysis of chromatographs of standard and sample solutions. Thus, k can be calculated.

Similarly, from the increasing of GGFL (the product) we have

$$k = \frac{A_p}{f_p \times [s]_i \times V_t \times t_s} \tag{14}$$

Appendix

List of Variables - Greek

ε_e extra particle porosity, 0.4

ε_i intraparticle porosity, 0.4

η viscosity of the mobile phase

λ numerical geometry-dependent constant, set to 2

$\sigma_{c,t}^2$ variance from a column in units of time squared

$\sigma_{r,t}^2$ variance from a CTR in the units of time squared

ϕ column permeability, set to 750

List of Variables - Roman

a_c column radius, set to 50 μm

a_r the radius of the capillary reactor

D diffusion coefficient of solute in mobile phase

d_p packing particle diameter

g numerical geometry-dependent constant, set to 30 (spherical particles)

H_0 the height equivalent to a theoretical plate without a CTR

H_c the height equivalent to a theoretical plate

H_r height equivalent to a theoretical plate in a CTR

k_0 constant, $k_0 = (1-\varepsilon_e)\varepsilon_i / \varepsilon_e$

k' the retention factor

k'' zone retention factor, $k'' = k_0 + (1+k_0)k'$

L_0 length of a column without a CTR

L_c length of a capillary column

L_r length of a CTR

N_{obs} observed number of theoretical plates from a column and a CTR

N_0 number of theoretical plates from a column alone

P_m maximum pressure provided by HPLC pump

T temperature

t_0 dead time of an ananlysis

u_0 average linear velocity in a column without a CTR

u_c average linear velocity in a column with a CTR

u_e exraparticle linear velocity

u_{e0} extraparticle linear velocity without a CTR

u_r linear velocity in the reactor

y a constant describing the degree of mixing by diffusion, set to 2.5